

Exploration of the Tensor Structure of the Higgs Boson Coupling to Weak Bosons in e^+e^- Collisions

Gilad Amar,^{1,2,*} Shankha Banerjee,^{3,†} Stefan von Buddenbrock,^{1,‡} Alan S. Cornell,^{2,§}
Tanumoy Mandal,^{3,¶} Bruce Mellado,^{1,**} and Biswarup Mukhopadhyaya^{3,††}

¹*School of Physics, University of the Witwatersrand, Wits 2050, South Africa*

²*National Institute for Theoretical Physics; School of Physics,
University of the Witwatersrand, Wits 2050, South Africa*

³*Regional Centre for Accelerator-based Particle Physics,
Harish-Chandra Research Institute, Chhatnag Road, Jhusi, Allahabad - 211019, India*

(Dated: November 7, 2021)

arXiv:1405.3957v3 [hep-ph] 16 Mar 2015

Abstract

Probing signatures of anomalous interactions of the Higgs boson with pairs of weak vector bosons is an important goal of an e^+e^- collider commissioned as a Higgs factory. We perform a detailed analysis of such potential of a collider operating at 250–300 GeV. Mostly using higher dimensional operators in a gauge-invariant framework, we show that substantial information on anomalous couplings can be extracted from the total rates of s - and t -channel Higgs production. The most obvious kinematic distributions, based on angular dependence of matrix elements, are relatively less sensitive with moderate coefficients of anomalous couplings, unless one goes to higher centre-of-mass energies. Some important quantities to use here, apart from the total event rates, are the ratios of event rates at different energies, ratios of s - and t -channel rates at fixed energies, and under some fortunate circumstances, the correlated changes in the rates for W -boson pair-production. A general scheme of calculating rates with as many as four gauge-invariant operators is also outlined. At the end, we perform a likelihood analysis using phenomenological parametrization of anomalous HWW interaction, and indicate their distinguishability for illustrative values of the strength of such interactions.

*Electronic address: gilad.amar@cern.ch

†Electronic address: shankha@hri.res.in

‡Electronic address: stefan.erich.von.buddenbrock@cern.ch

§Electronic address: alan.cornell@wits.ac.za

¶Electronic address: tanumoymandal@hri.res.in

**Electronic address: bmellado@mail.cern.ch

††Electronic address: biswarup@hri.res.in

I. INTRODUCTION

Physicists are widely convinced now that they have discovered what closely resembles the Higgs boson [1, 2] postulated in the standard electroweak model (SM) [3–11]. Along with widespread exhilaration, such a development brings in questions on whether this particle carries some signature of physics beyond the standard model. Many studies in this direction have appeared [12–56] in the context of the Large Hadron Collider (LHC) where the data available so far still allow some departure from SM behaviour. Even a finite invisible branching ratio (BR) for the Higgs cannot, at the moment, be ruled out [57, 58]. The issue can be probed through careful measurements of the couplings of the Higgs (or Higgs-like scalar) to various pairs of SM particles. Among them, the couplings to pairs of vector bosons (HVV) are measured in a relatively more reliable manner. This possibility has been explained in the context of an ep collider too [59, 60].

In view of the cumulative demand for a closer probe on the HVV couplings (and of course the couplings to other SM particles), the most desirable endeavour, however, is to build an electron-positron collider which provides a clean environment for precise measurements of Higgs interaction strengths. The first step is of course to develop a Higgs factory (at $\sqrt{s} \approx 250 - 300$ GeV). Such a machine will not only produce the Higgs boson copiously near resonance, but is also the first step before an e^+e^- machine at even higher energies is developed. In this paper, we incorporate some observations regarding the signatures of anomalous HVV couplings, manifest through higher dimensional operators (HDOs), at a Higgs factory. Other studies performed for an e^+e^- machine can be found in [61].

If the couplings arise through physics at a scale higher than that of electroweak symmetry breaking, then the resulting higher-dimensional effective interactions are expected to be gauge invariant. Such interactions have not only been identified, but constraints on their coefficients have also been obtained from the LHC data [52, 62–66]. In view of such analyses, the coefficients are often restricted to such values where many cherished kinematic distributions may fail to reveal their footprints. In the current study, we point out some features which influence the detectability (or otherwise) of the higher-dimensional couplings at a Higgs factory. At the same time, we emphasise some possible measurements that can elicit their signatures even for relatively small coefficients of such operators.

We concentrate on two Higgs production channels, namely, $e^+e^- \rightarrow ZH$ (the s -channel

process) and $e^+e^- \rightarrow \nu\bar{\nu}H$ (the t -channel process, which we separate with the help of a simple kinematic cut around the Higgs boson energy). In principle, the HDOs that will constitute our report can influence the rates in both channels. In contrast, the most obvious kinematic distributions, namely, those based on the angular dependence of matrix elements, drawn with moderate values of their coefficients do not show a perceptible difference with respect to the SM situation. Keeping this in view, we underscore the following points here:

1. The s -channel process has substantial rates at ≤ 300 GeV or thereabout. We show, through an analysis of the production amplitude squared, why one cannot expect significantly different angular distributions in this channel at such energies, if one uses moderate values of the operator coefficients.
2. The t -channel process can have appreciable production rates at high energies (\approx a TeV), too. Because of the production of two neutrinos in the final state, this process provides limited phase-space for the exploration of the tensor structure of the HWW coupling. Here it is attempted to exploit the full kinematics of the Higgs boson by means of a correlated two-dimensional likelihood analysis.
3. We show that, given such impediment, it is possible to uncover signatures of the aforementioned BSM operators through measurements of rates at two different energies, which also cancels many systematic uncertainties. In general, the energy dependence of the rates can be sensitive to anomalous couplings.
4. The very fact that the additional operators should be electroweak gauge invariant imply not only higher-dimensional HVV interactions ($V = W, Z, \gamma$) but also anomalous WWV interactions ($V = Z, \gamma$) whose strengths are related to the former. We show that the concomitant variations in Higgs production and W-pair production at Higgs factories may elicit the presence of such BSM interactions.
5. We also show that if the centre-of-mass energy (CME) of the colliding particles is ≈ 500 GeV or more, then even moderate values of the operator coefficients can show some differences in the kinematic distributions.
6. Lastly, we perform the analysis in a framework that allows one to retain all the gauge-invariant operators at the same time.

We summarise the gauge invariant couplings in the next section, and subsequently point out the ‘phenomenological’ anomalous couplings they lead to. In section III, we take up the s and t -channel Higgs production cross-sections in turn, and explain why one cannot expect too much out of kinematic distributions at Higgs factory energies, so long as the BSM coupling coefficients are subject to constraints imposed by the LHC data. Their detectable signatures through event ratios at two energies, and also via the simultaneous measurement of W -pair production are predicted in section III. A likelihood analysis and some related issues, mostly in terms of the phenomenological forms to which all new couplings reduce, are found in section IV. We summarise our conclusions in section V.

II. EFFECTIVE LAGRANGIAN FORMALISM

In this paper, we adopt two types of effective Lagrangian parametrizations which are commonly used in the literature to probe the anomalous HVV (where $V = W, Z, \gamma$) interactions. In one parametrization, we take the most general set of dimension-6 gauge invariant operators which give rise to such anomalous HVV interactions. In the other one, we parametrize the HVV vertices with the most general Lorentz invariant structure. Although, this formalism is not the most transparent one from the viewpoint of the gauge structure of the theory, it is rather simple and more experiment-friendly. Both formalisms modify the HVV vertices by introducing non-standard momentum-dependent terms.

We assume that the SM is a low-energy effective theory of a more complete perturbation theory valid below a cut-off scale Λ . In the present study, we are concerned mainly with the Higgs sector. The first order corrections to the Higgs sector will come from gauge invariant dimension 6 operators as there is only one dimension-5 operator which contributes to the neutrino masses. The relevant additional Lorentz structures in HVV interactions are necessarily of dimensions higher than four. If they arise as a consequence of integrating out physics at a higher scale, all such operators will have to be invariant under $SU(2)_L \times U(1)_Y$. A general classification of such operators is found in the literature [67–70]. The lowest order CP-conserving operators which are relevant for Higgs phenomenology are

- The operators containing the Higgs doublet Φ and its derivatives:

$$\mathcal{O}_{\Phi,1} = (D_\mu \Phi)^\dagger \Phi \Phi^\dagger (D^\mu \Phi); \quad \mathcal{O}_{\Phi,2} = \frac{1}{2} \partial_\mu (\Phi^\dagger \Phi) \partial^\mu (\Phi^\dagger \Phi); \quad \mathcal{O}_{\Phi,3} = \frac{1}{3} (\Phi^\dagger \Phi)^3 \quad (1)$$

- The operators containing the Higgs doublet Φ (or its derivatives) and bosonic field strengths :

$$\mathcal{O}_{GG} = \Phi^\dagger \Phi G_{\mu\nu}^a G^{a\mu\nu}; \quad \mathcal{O}_{BW} = \Phi^\dagger \hat{B}_{\mu\nu} \hat{W}^{\mu\nu} \Phi; \quad \mathcal{O}_{WW} = \Phi^\dagger \hat{W}_{\mu\nu} \hat{W}^{\mu\nu} \Phi$$

$$\mathcal{O}_W = (D_\mu \Phi)^\dagger \hat{W}^{\mu\nu} (D_\nu \Phi); \quad \mathcal{O}_{BB} = \Phi^\dagger \hat{B}_{\mu\nu} \hat{B}^{\mu\nu} \Phi; \quad \mathcal{O}_B = (D_\mu \Phi)^\dagger \hat{B}^{\mu\nu} (D_\nu \Phi), \quad (2)$$

where $\hat{W}^{\mu\nu} = i \frac{g}{2} \sigma_a W^{a\mu\nu}$ and $\hat{B}^{\mu\nu} = i \frac{g'}{2} B^{\mu\nu}$ and g, g' are respectively the $SU(2)_L$ and $U(1)_Y$ gauge couplings. $W_{\mu\nu}^a = \partial_\mu W_\nu^a - \partial_\nu W_\mu^a - g \epsilon^{abc} W_\mu^b W_\nu^c$, $B_{\mu\nu} = \partial_\mu B_\nu - \partial_\nu B_\mu$ and $G_{\mu\nu}^a = \partial_\mu G_\nu^a - \partial_\nu G_\mu^a - g_s f^{abc} G_\mu^b G_\nu^c$. The Higgs doublet is denoted by Φ and its covariant derivative is given as $D_\mu \Phi = (\partial_\mu + \frac{i}{2} g' B_\mu + i g \frac{\sigma_a}{2} W_\mu^a) \Phi$.

Following are the properties of the aforementioned HDOs:

- $\mathcal{O}_{\Phi,1}$: Does not preserve custodial symmetry and is therefore severely constrained by the T -parameter (or equivalently the ρ parameter). It modifies the SM HZZ and HWW couplings by unequal multiplicative factors.
- $\mathcal{O}_{\Phi,2}$: Preserves custodial symmetry and modifies the SM HZZ and HWW couplings by multiplicative factors. This operator modifies the Higgs self-interaction as well.
- $\mathcal{O}_{\Phi,3}$: Modifies only the Higgs self-interaction.
- \mathcal{O}_{GG} : Introduces HGG coupling which is same in structure as the SM effective HGG coupling. Since our discussion is limited to the context of an e^+e^- collider and as we will also not consider the gluonic decay mode of the Higgs, we will not discuss this operator any further.
- \mathcal{O}_{BW} : Drives the tree-level $Z \leftrightarrow \gamma$ mixing and is therefore highly constrained by the electroweak precision test (EWPT) data [62].
- $\mathcal{O}_{WW}, \mathcal{O}_W, \mathcal{O}_{BB}, \mathcal{O}_B$: Modifies the HVV couplings by introducing new Lorentz structure in the Lagrangian. They are not severely constrained by the EWPT data[63, 64].

Hence for the Higgs sector, we will choose our basis as $\mathcal{O}_i \in \{\mathcal{O}_{WW}, \mathcal{O}_W, \mathcal{O}_{BB}, \mathcal{O}_B\}$. In the presence of the above operators, the Lagrangian is parametrised as

$$\mathcal{L} = \kappa \left(\frac{2m_W^2}{v} HW_\mu^+ W^{\mu-} + \frac{m_Z^2}{v} H Z_\mu Z^\mu \right) + \sum_i \frac{f_i}{\Lambda^2} \mathcal{O}_i \quad (3)$$

where κ is the scale factor of the SM-like coupling, something which needs to be accounted for when considering BSM physics. f_i is a dimensionless coefficient which denotes the strength of the i^{th} operator and Λ is the cut-off scale above which new physics must appear. We keep κ to be the same for the HWW and HZZ couplings so that there is no unacceptable contribution to the ρ -parameter. Another operator considered in this work is $\mathcal{O}_{WWW} = Tr[\hat{W}_{\mu\nu}\hat{W}^{\nu\rho}\hat{W}_\rho^\mu]$. This only affects the triple gauge boson couplings and does not affect the Higgs sector.

The effective Lagrangian which affects the Higgs sector is

$$\begin{aligned}\mathcal{L}_{eff} &= g_{HWW}^{(1)} (W_{\mu\nu}^+ W^{-\mu} \partial^\nu H + h.c.) + g_{HWW}^{(2)} HW_{\mu\nu}^+ W^{-\mu\nu} \\ &+ g_{HZZ}^{(1)} Z_{\mu\nu} Z^\mu \partial^\nu H + g_{HZZ}^{(2)} HZ_{\mu\nu} Z^{\mu\nu} \\ &+ g_{HZ\gamma}^{(1)} A_{\mu\nu} Z^\mu \partial^\nu H + g_{HZ\gamma}^{(2)} HA_{\mu\nu} Z^{\mu\nu} + g_{H\gamma\gamma} HA_{\mu\nu} A^{\mu\nu},\end{aligned}\quad (4)$$

where

$$\begin{aligned}g_{HWW}^{(1)} &= \left(\frac{gM_W}{\Lambda^2}\right) \frac{f_W}{2}; & g_{HWW}^{(2)} &= -\left(\frac{gM_W}{\Lambda^2}\right) f_{WW} \\ g_{HZZ}^{(1)} &= \left(\frac{gM_W}{\Lambda^2}\right) \frac{c^2 f_W + s^2 f_B}{2c^2}; & g_{HZZ}^{(2)} &= -\left(\frac{gM_W}{\Lambda^2}\right) \frac{s^4 f_{BB} + c^4 f_{WW}}{2c^2} \\ g_{HZ\gamma}^{(1)} &= \left(\frac{gM_W}{\Lambda^2}\right) \frac{s(f_W - f_B)}{2c}; & g_{HZ\gamma}^{(2)} &= \left(\frac{gM_W}{\Lambda^2}\right) \frac{s(s^2 f_{BB} - c^2 f_{WW})}{c} \\ g_{H\gamma\gamma} &= -\left(\frac{gM_W}{\Lambda^2}\right) \frac{s^2(f_{BB} + f_{WW})}{2}\end{aligned}\quad (5)$$

with $s(c)$ being the sine (cosine) of the Weinberg angle. The operators \mathcal{O}_W , \mathcal{O}_B and \mathcal{O}_{WWW} contribute to the anomalous triple gauge boson interactions. The interactions can be summarised as

$$\mathcal{L}_{WWV} = -ig_{WWV} \left\{ g_1^V (W_{\mu\nu}^+ W^{-\mu} V^\nu - W_\mu^+ V_\nu W^{-\mu\nu}) + \kappa_V W_\mu^+ W_\nu^- V^{\mu\nu} + \frac{\lambda_V}{M_W^2} W_{\mu\nu}^+ W^{-\nu\rho} V_\rho^\mu \right\},\quad (6)$$

where $g_{WW\gamma} = g s$, $g_{WWZ} = g c$, $\kappa_V = 1 + \Delta\kappa_V$ and $g_1^Z = 1 + \Delta g_1^Z$ with

$$\begin{aligned}\Delta\kappa_\gamma &= \frac{M_W^2}{2\Lambda^2} (f_W + f_B); & \lambda_\gamma = \lambda_Z &= \frac{3g^2 M_W^2}{2\Lambda^2} f_{WWW} \\ \Delta g_1^Z &= \frac{M_W^2}{2c^2 \Lambda^2} f_W; & \Delta\kappa_Z &= \frac{M_W^2}{2c^2 \Lambda^2} (c^2 f_W - s^2 f_B)\end{aligned}\quad (7)$$

The limits on these operators have been derived in many references. The most comprehensive of these are listed in references [52, 62–65]. These operators, even within their

current limits, have been shown to modify the efficiencies of the various selection cuts for the relevant final states in the context of the LHC [66].

All of the aforementioned HDOs lead essentially to one effective coupling (each for HWW and HZZ), when CP -violation is neglected. These can be alternatively used in a phenomenological way for example, the $H(k)W_\mu^+(p)W_\nu^-(q)$ vertex can be parametrised as [71]:

$$i\Gamma^{\mu\nu}(p, q)\epsilon_\mu(p)\epsilon_\nu^*(q), \quad (8)$$

where deviations from the SM form of $\Gamma_{SM}^{\mu\nu}(p, q) = -gM_W g^{\mu\nu}$ would indicate the presence of BSM physics. These BSM deviations, including CP -violating ones (not considered among the gauge invariant operators), can be specified as

$$\Gamma_{\mu\nu}^{BSM}(p, q) = \frac{g}{M_W}[\lambda(p \cdot q g_{\mu\nu} - p_\nu q_\mu) + \lambda' \epsilon_{\mu\nu\rho\sigma} p^\rho q^\sigma], \quad (9)$$

where λ and λ' are the effective strengths for the anomalous CP -conserving and CP -violating operators respectively.

Precise identification of the non-vanishing nature of λ, λ' is a challenging task. If ever accomplished, it can tell us whether the modification in HVV -couplings are CP -conserving or CP -violating in nature and, if both are present, what their relative proportion is. Here we analyse the process $e^+e^- \rightarrow H\nu\bar{\nu}$ and see if there is any BSM physics involved by incorporating a likelihood analysis of the SM hypothesis tested against BSM hypotheses.

A few comments are in order on the two ways of parametrizing the anomalous Higgs couplings. The latter, of course, encapsulates all possible modified Lorentz invariant couplings in the lowest possible order, including both CP -conserving and CP -violating ones, in the coefficients λ and λ' respectively. All of the anomalous HWW and HZZ couplings listed in the gauge-invariant formulation reduce basically to one term if one confines oneself to a CP -conserving scenario. Thus we can say that the latter parametrization shows us a rather ‘economic’ way of relating the anomalous HVV interactions to collider phenomenology. On the other hand, the process of relating the anomalous couplings to specific effective interactions is more transparent from the viewpoint of gauge structures when one uses the gauge invariant HDOs. It paves an easier path towards understanding the ultraviolet completion of the scenario. In addition to this, the formulation in terms of gauge-invariant operators relates the anomalous HWW and HZZ interactions. One finds, in this way, a pattern in the departure of the ZH and $\nu\bar{\nu}H$ final state production rates from the corresponding SM

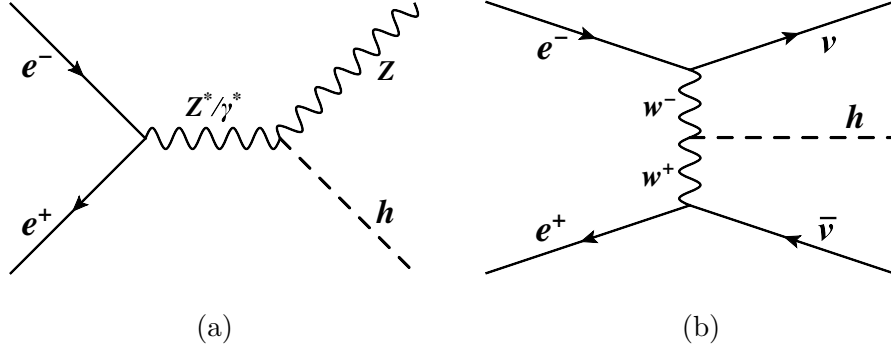


FIG. 1: (a) s -channel Feynman diagrams (b) t -channel Feynman Diagram.

prediction. Finally, some of the gauge-invariant operators lead simultaneously to anomalous triple gauge boson interactions. There is thus an associated variation in the ZH , $\nu\bar{\nu}H$ and W^+W^- production rates as well as in the kinematic distributions associated with each final state. Such an association enables one to use various pieces of data to determine each new operator.

III. PHENOMENOLOGY AT AN e^+e^- COLLIDER

In this section, we discuss various important Higgs production mechanisms through HVV vertices at an e^+e^- collider. For the collider phenomenology, we have implemented the Lagrangians of Eqs. (4) and (6) in `FeynRules` [72] to generate `Universal FeynRules Model (UFO)` [73] files suitable for interfacing with `MadGraph` [74]. We also use `FORM` [75] to compute many cross-sections analytically.

A. Higgs production at an e^+e^- collider

We concentrate on two main Higgs production mechanisms *viz.* $e^+e^- \rightarrow ZH$ and $e^+e^- \rightarrow \nu\bar{\nu}H$, at an e^+e^- collider with energies ranging from 250 GeV to 500 GeV. The $e^+e^- \rightarrow ZH$ channel includes only the s -channel processes – $e^+e^- \rightarrow Z^*/\gamma^* \rightarrow ZH$ (shown in Fig. 1(a)). Whereas $e^+e^- \rightarrow \nu\bar{\nu}H$ includes both the s -channel processes, $e^+e^- \rightarrow Z^*/\gamma^* \rightarrow ZH \rightarrow \nu\bar{\nu}H$ as well as the t -channel process $e^+e^- \rightarrow \nu\bar{\nu}W^*W^* \rightarrow \nu\bar{\nu}H$ (WW fusion process as shown in Fig. 1(b)).

The s and t -channel processes have different kinematics and hence are affected differently by the inclusion of the HDOs. Moreover, the t -channel process allows us to explore the

tensor structure of the $HW\bar{W}$ vertex alone, free from any contamination from the HZZ and $HZ\gamma$ vertices. On the other hand, the s -channel process is free from any contamination due to the $HW\bar{W}$ vertex. Hence, the measurement of the s -channel contribution will shed light on the tensorial nature of the HZZ and $HZ\gamma$ vertices. We, therefore, analyse the s and t -channel processes separately to shed more light on the anomalous behaviour of the HVV vertices. We separate the s -channel (t -channel) contribution from the $e^+e^- \rightarrow \nu\bar{\nu}H$ events by applying a simple kinematic cut on the Higgs energy (E_H) as follows:

$$E_H\text{-cut: } \left| E_H - \frac{s + M_H^2 - M_Z^2}{2\sqrt{s}} \right| \leq \Delta \quad \left(E_H^c\text{-cut: } \left| E_H - \frac{s + M_H^2 - M_Z^2}{2\sqrt{s}} \right| \geq \Delta \right), \quad (10)$$

where \sqrt{s} is the CME of the two colliding e^+e^- beams and Δ is an energy-window around E_H . Here, E_H^c -cut is complementary to the E_H -cut. We use $\Delta = 5$ GeV throughout our analysis¹. We must mention here that for the rest of this paper the s -channel process will be studied at the ZH level without any cuts, unless otherwise specified. One can easily get an estimate of the cross-section for any decay modes of Z by multiplying the appropriate BR. This is because for the $e^+e^- \rightarrow l^+l^-H$ channel, a simple invariant mass cut on the two leptons about the Z boson mass will separate the s -channel to a very high degree. For $e^+e^- \rightarrow \nu\bar{\nu}H$, on the other hand, the cut on E_H separates the s and t -channels. The s -channel contribution surviving the cut is found to be very close to what one would have found from the rate for l^+l^-H , through a scaling of BRs. One is thus confident that the E_H -cut is effective in minimising mutual contamination of the s and t -channel contributions.

It should also be mentioned here that the effects of beam energy spread are not taken into account in Eq. 10 for simplification. While we present the basic ideas of distinguishing anomalous interactions of the Higgs, the relevant energy window for precision studies has to factor in the effects of bremsstrahlung as well as beamstrahlung (depending on whether the Higgs factory is a circular or a linear collider).

In Table I, we show the effect of the E_H -cut on the $\nu\bar{\nu}H$ channel in the SM and in presence of HDOs for one benchmark point, BP1 ($\kappa = 1, f_{WW} = -3, f_W = 8, f_{BB} = -4, f_B = 3$) which closely mimics the SM cross-section. The E_H -cut keeps almost all the s -

¹ Typical values of Δ can be estimated from the energy uncertainties of the b -jets coming from the Higgs decay. The jet energy uncertainty ΔE_{jet} (1σ) of a jet having energy E_{jet} are related as, $\Delta E_{jet}/E_{jet} \lesssim 0.3/\sqrt{E_{jet}}$ at the ILC [76]. For example, if there are two b -jets each with energy 100 GeV, the total uncertainty in their energy measurement is $\sqrt{2 \times (0.3 \times \sqrt{100})^2} \sim 4$ GeV (added in quadrature).

\sqrt{s} (GeV)	Benchmark point	$\sigma_{\nu\bar{\nu}H}^{tot}$ (fb)	$\sigma_{\nu\bar{\nu}H}^s$ (fb)	$\sigma_{\nu\bar{\nu}H}^t$ (fb)	$\sigma_{\nu\bar{\nu}H}^{int}$ (fb)	$\sigma_{\nu\bar{\nu}H}^{s,ac}$ (fb)	$\sigma_{\nu\bar{\nu}H}^{t,ac}$ (fb)
300	SM	52.43	36.35	17.83	-1.75	37.24	15.19
	BP1	52.11	35.29	18.83	-2.01	36.76	15.35
500	SM	84.80	11.64	74.07	-1.11	11.93	72.83
	BP1	87.38	7.37	81.50	-1.49	7.83	79.55

TABLE I: We show the total $\nu\bar{\nu}H$ cross-section ($\sigma_{\nu\bar{\nu}H}^{tot}$), only s -channel cross-section ($\sigma_{\nu\bar{\nu}H}^s$), only t -channel cross-section ($\sigma_{\nu\bar{\nu}H}^t$) and their interference contribution ($\sigma_{\nu\bar{\nu}H}^{int}$) for the SM ($\kappa = 1, f_{WW} = 0, f_W = 0, f_{BB} = 0, f_B = 0$) and for HDO benchmark point BP1 ($\kappa = 1, f_{WW} = -3, f_W = 8, f_{BB} = -4, f_B = 3$) for two different CMEs. We also present the s ($\sigma_{\nu\bar{\nu}H}^{s,ac}$) and t -channel ($\sigma_{\nu\bar{\nu}H}^{t,ac}$) cross-sections separated from the $\nu\bar{\nu}H$ events after applying the cut defined in Eq. 10. The superscript ac means after cut.

channel contribution but the E_H^c -cut cuts out a small portion around E_H from the t -channel contribution. Therefore, the s -channel cross-sections after this cut increase slightly from their without-cut values due to this small t -channel contamination. On the other hand, the t -channel cross-sections after cut decrease slightly from their without-cut values. We also estimate the interference between the s and t -channel diagrams and present the numbers in Table I. Interference contribution is expected to be tiny in the \sqrt{s} region sufficiently away from the s -channel threshold energy ($M_H + M_Z$) ≈ 226 GeV. We find that the interference contribution is only $\sim 3.5\%$ of the total cross-section for $\sqrt{s} = 300$ GeV, in the SM. This reaffirms the statement at the end of the previous paragraph. We also note that the inclusion of HDOs with moderate values of coefficients does not affect this contribution much. Hence, by neglecting the interference term, we approximate the total $\nu\bar{\nu}H$ cross-section as

$$\sigma_{\nu\bar{\nu}H}^{tot} \approx \sigma_{ZH} \times BR_{Z \rightarrow \nu\bar{\nu}} + \sigma_{\nu\bar{\nu}H}^t, \quad (11)$$

where σ_{ZH} is the s -channel cross section and $BR_{Z \rightarrow \nu\bar{\nu}}$ is the invisible branching fraction ($\approx 20\%$) of the Z -boson.

Fig. 2 shows the invariant mass distribution of the neutrino pair for the process $e^+e^- \rightarrow \nu\bar{\nu}H$ at $\sqrt{s} = 300$ GeV and for the benchmark point BP1. We separately show the distributions for the total process (which includes the s and t channels as well as the interference) and also the s and t channels separately. In an inset plot we show the distribution due to this

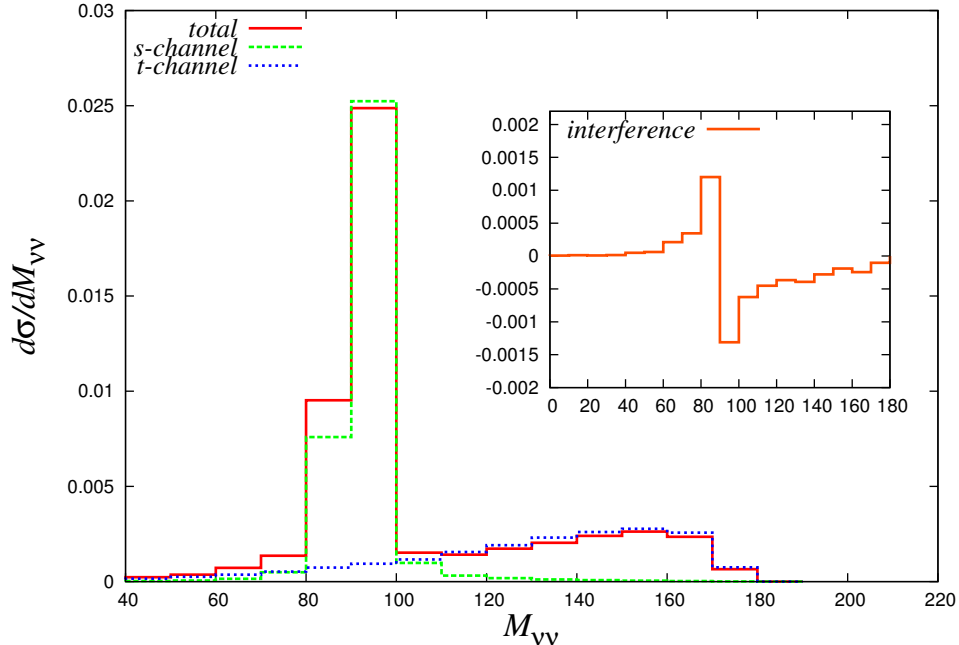


FIG. 2: Invariant mass distributions of $\nu\bar{\nu}$ of the process $e^+e^- \rightarrow \nu\bar{\nu}H$ at $\sqrt{s} = 300$ GeV and for the benchmark point BP1 ($\kappa = 1, f_{WW} = -3, f_W = 8, f_{BB} = -4, f_B = 3$). The red, green, blue histograms are for the total ($s + t + \text{interference}$), s and t channels respectively. The inset (orange) plot shows the interference ($\text{total} - s - t$) contribution.

interference. This clearly shows that it is negligible when compared to the s and t channel contributions. This nature generally holds for the parameter space under consideration.

B. A general expression for the cross-sections

In this analysis, we keep $\kappa, f_{WW}/\text{TeV}^2, f_W/\text{TeV}^2, f_{BB}/\text{TeV}^2$ and f_B/TeV^2 as free parameters. The HWW vertex depends on three parameters (κ, f_{WW} and f_W) whereas the HZZ and the $HZ\gamma$ vertices depend on five parameters ($\kappa, f_{WW}, f_W, f_{BB}$ and f_B). The κ dependence enters the $HZ\gamma$ vertex through the W -loop in the effective $HZ\gamma$ vertex. The amplitude for the process $e^+e^- \rightarrow ZH/\nu\bar{\nu}H$ is a linear combination of $x_i \in \{\kappa, f_{WW}, f_W, f_{BB}, f_B\}$ and therefore, the cross-section can always be expressed as a bi-linear form, $\sigma(S, x_i) = \sum_{i,j=1}^5 x_i C_{ij}(S) x_j$, where $C_{ij}(S)$ is the ij^{th} element of the coefficient matrix $\mathcal{M}(\sqrt{s})$ at a CME of \sqrt{s} . Hence, the cross-section can be written in the following

closed form

$$\sigma(\sqrt{s}) = \mathcal{X} \cdot \mathcal{M}(\sqrt{s}) \cdot \mathcal{X}^T, \quad (12)$$

where $\mathcal{X} = (\kappa, f_{WW}, f_W, f_{BB}, f_B)$ is a row vector.

The matrices of coefficients for the $e^+e^- \rightarrow ZH$ process at $\sqrt{s} = 250$ GeV and 300 GeV are

$$\mathcal{M}_{250}^{s,ZH} = \begin{pmatrix} 241.32 & -7.11 & -2.29 & -0.55 & -0.51 \\ -7.11 & 0.35 & 0.13 & -0.02 & -0.05 \\ -2.29 & 0.13 & 0.06 & -0.01 & -0.03 \\ -0.55 & -0.02 & -0.01 & 0.01 & 0.02 \\ -0.51 & -0.05 & -0.03 & 0.02 & 0.04 \end{pmatrix}; \mathcal{M}_{300}^{s,ZH} = \begin{pmatrix} 181.67 & -6.43 & -2.99 & -0.51 & -0.71 \\ -6.43 & 0.46 & 0.18 & -0.03 & -0.08 \\ -2.99 & 0.18 & 0.14 & -0.02 & -0.06 \\ -0.51 & -0.03 & -0.02 & 0.02 & 0.03 \\ -0.71 & -0.08 & -0.06 & 0.03 & 0.08 \end{pmatrix} \quad (13)$$

Similar matrices for the t -channel process (after the E_H^c -cut) for the channel $e^+e^- \rightarrow \nu\bar{\nu}H$ at $\sqrt{s} = 250$ GeV and 300 GeV are

$$\mathcal{M}_{250}^{t,\nu\bar{\nu}H} = \begin{pmatrix} 4.63 & 5.2 \times 10^{-3} & 0.02 \\ 5.2 \times 10^{-3} & 2.9 \times 10^{-4} & -1.2 \times 10^{-4} \\ 0.02 & -1.2 \times 10^{-4} & 1.6 \times 10^{-4} \end{pmatrix}; \mathcal{M}_{300}^{t,\nu\bar{\nu}H} = \begin{pmatrix} 15.36 & 0.04 & 0.07 \\ 0.04 & 1.2 \times 10^{-3} & -7.7 \times 10^{-4} \\ 0.07 & -7.7 \times 10^{-4} & 4.6 \times 10^{-4} \end{pmatrix} \quad (14)$$

We must mention here that the matrices in Eq. 14 are three-dimensional compared to the five-dimensional matrices in Eq. 13 because the t -channel only involves the HWW vertex which is not affected by the operators \mathcal{O}_{BB} and \mathcal{O}_B (Eqs. 4, 5). We also observe that in Eq. 13, the coefficients of the matrix related to either f_{BB} or f_B are much less pronounced compared to the coefficients involving the other three parameters, *viz.* κ , f_{WW} and f_W . Also from Eq. 14 we see that barring the (1,1) entry in the matrices, all the other coefficients are small implying that the HDOs will have small but non-negligible effects on the t -channel cross-sections for energies at the Higgs factories.

An explanation of relatively less dependence of the t -channel cross-section compared to the s -channel on the anomalous operators can also be understood from Fig. 3. The plots reveal that, for the former process (essentially a vector boson fusion channel), the Higgs emerges with much smaller energy. The higher-dimensional couplings, on the other hand, contain derivatives which translate into a direct dependence on the energy of the Higgs,

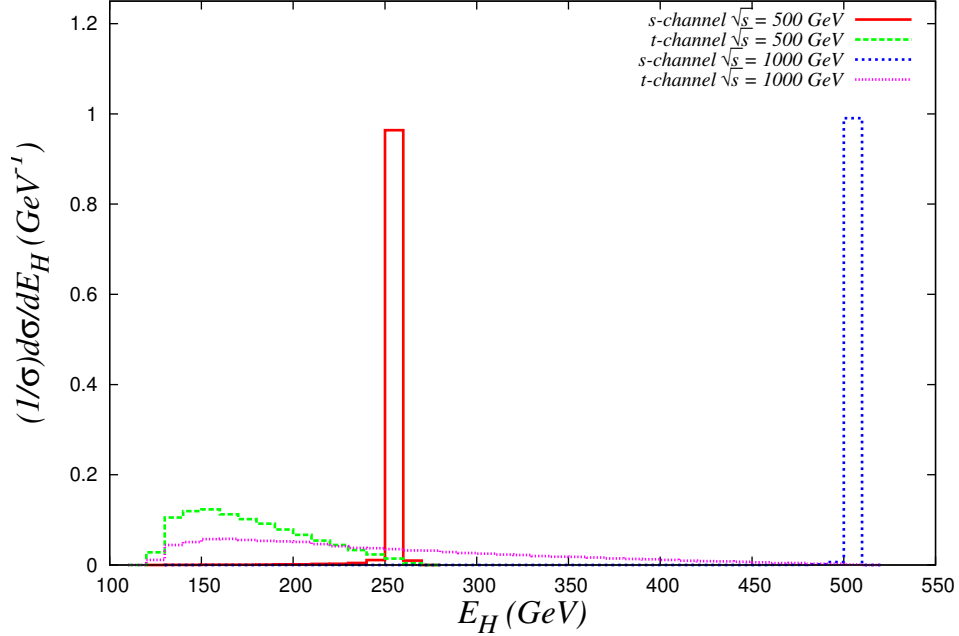


FIG. 3: Normalised distributions of the Higgs energy (E_H) for the s -channel (red : $\sqrt{s} = 500$ GeV and blue : $\sqrt{s} = 1$ TeV) and t -channel (green : $\sqrt{s} = 500$ GeV and magenta : $\sqrt{s} = 1$ TeV) for the benchmark point BP1.

thus putting the t -channel process at a relative disadvantage. The Higgs energy distribution shows a longer tail for higher centre-of-mass energies, thus offering a partial recompense to the t -channel process for an energy as high as a TeV.

In this study we also consider the process $e^+e^- \rightarrow W^+W^-$ which involves the triple-gauge boson vertices $WW\gamma$ and WWZ . These are concomitantly affected by the operators \mathcal{O}_W and \mathcal{O}_B . Besides, as mentioned in section II, such vertices are also affected by the operator \mathcal{O}_{WWW} which does not affect the Higgs sector. In the basis of $x_i^{WW} \in \{1, f_W, f_B, f_{WWW}\}$, the coefficient matrix at $\sqrt{s} = 300$ GeV is given by

$$\mathcal{M}_{300}^{WW} = \begin{pmatrix} 13.48 & 1.10 \times 10^{-2} & 5.65 \times 10^{-3} & 4.24 \times 10^{-3} \\ 1.10 \times 10^{-2} & 4.98 \times 10^{-4} & 5.27 \times 10^{-5} & 2.02 \times 10^{-4} \\ 5.65 \times 10^{-3} & 5.27 \times 10^{-5} & 1.17 \times 10^{-4} & 1.96 \times 10^{-5} \\ 4.24 \times 10^{-3} & 2.02 \times 10^{-4} & 1.96 \times 10^{-5} & 8.18 \times 10^{-4} \end{pmatrix}. \quad (15)$$

As we can see above, all the C_{ij} s are very small when compared to C_{11} , which gives us the SM cross-section. We will discuss this channel in more details later in this paper.

C. Energy dependence of s and t -channel cross-sections

It is well-known that in SM, the cross-section for the s -channel falls with the CME as $1/S$ and that for the t -channel, rises as $\ell n S$ [77]. However, for sets of values of our parameters, different from the SM, the nature of the s -channel curve can be completely different from its SM-counterpart. The t -channel cross-section however is not affected so significantly on the introduction of HDOs as has been discussed in detail in the previous sub-section. We show the variation of the s and t -channel processes for \sqrt{s} ranging from 250 GeV to 900 GeV. In contrast to the SM nature of a fall in the s -channel cross-section with energy, the introduction of HDOs does in no way ensure such a nature which can be seen in Fig.4 (a) for two benchmark points (BP2 ($x_i \in \{1, 0, 5, 0, 0\}$) and BP3 ($x_i \in \{1, 0, -5, 0, 0\}$)) alongside the SM. The above two benchmark points have been chosen as the cross-sections are quite sensitive to f_W and the two points are allowed from EWPT constraints. On the whole it is clear from the diagrams that the ratio of the s and t -channel cross-sections in some channel at a particular energy can be an important probe to the nature of new Higgs couplings²

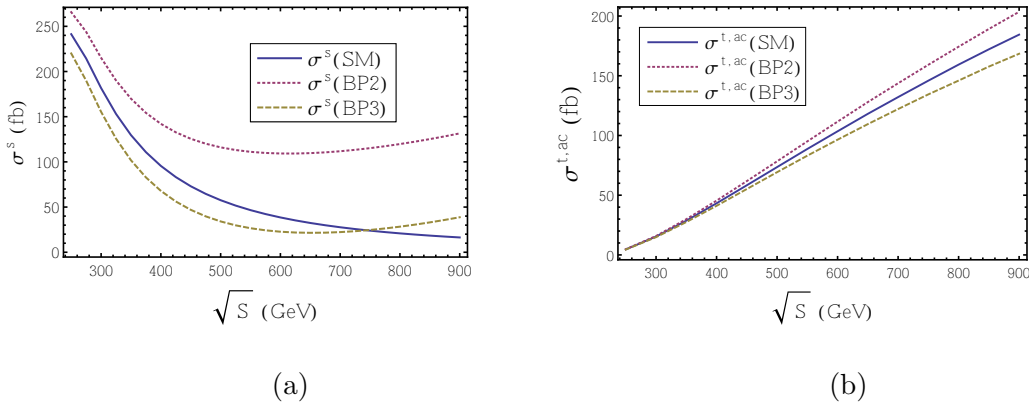


FIG. 4: (a) : σ^s (in fb) for the channel $e^+e^- \rightarrow ZH$ and (b) : $\sigma^{t,ac}$ (in fb) for the channel $e^+e^- \rightarrow \nu\bar{\nu}H$ as functions of the CME, \sqrt{s} . The cross-sections have been computed for three benchmark points, viz. SM ($x_i \in \{1, 0, 0, 0, 0\}$), BP2 ($x_i \in \{1, 0, 5, 0, 0\}$) and BP3 ($x_i \in \{1, 0, -5, 0, 0\}$). The superscript ac denotes the after cut scenario.

² The visible rise with \sqrt{s} (in Fig.4(a) for the benchmark points BP2 and BP3) does not threaten unitarity, since the additional degrees of freedom responsible for the effective operators take care of it when \sqrt{s} approaches Λ . The rise is not noticeable if one has the operators $\mathcal{O}_{WW}/\mathcal{O}_{BB}$ instead of $\mathcal{O}_W/\mathcal{O}_B$. The different momentum dependence in the former case tames the rise with \sqrt{s} as can be verified from the corresponding Feynman rules in [70].

D. More information from the total rates

The total rates and their ratios at different CMEs can be important probes to identify the tensor structure of the HVV couplings. We show how the total rates for the s and t -channel processes are affected on the introduction of the effective operators (Eqs. 13 and 14).

We must make a statement about the values of the coefficients, f_i/Λ^2 (i is the index of the operator under consideration) chosen in the rest of the paper. In most cases, f_i/Λ^2 is allowed to vary in the range $[-20, 20]$ TeV^{-2} . Now, a reasonable criterion for the validity of the effective field theory [78] is $f_i x(g) E^2/\Lambda^2 < 1$, where $x(g)$ are the $SU(2)_L/U(1)_Y$ factors for the operators under study and E is the scale of the process. For the production case, it is the centre of mass energy of the e^+e^- colliding beams, which is 250 – 300 GeV, while for decays, it is the mass of the Higgs boson. For the production case, we perform a rough calculation taking $g \approx 0.65$, $g' \approx 0.74$ and the cut-off scale $\Lambda = 1$ TeV. Hence, for the operator \mathcal{O}_W , $f_W x(g) E^2/\Lambda^2 \approx f_W \frac{0.65}{2} 300^2/1000^2 \approx 0.029 f_W$, which can take f_W to values $\simeq 34$. Similarly, for \mathcal{O}_B , the reach will be around $f_B \simeq 30$. For \mathcal{O}_{WW} , we have two factors of g and two factors of $\frac{1}{2}$, which can take f_{WW} to an even larger value. Thus the values chosen in our scan approximately conforms to the requirement of a valid effective theory.

1. One parameter at a time

In Figs. 5 and 6, we show the variations of the $e^+e^- \rightarrow ZH$ and $e^+e^- \rightarrow \nu\bar{\nu}H$ (t -channel) cross-sections as functions of a single parameter by keeping all other parameters fixed at their SM values. We show that even for small values of the operator coefficients, the cross-sections can vary significantly from the SM expectations. We also show that the ratios of the cross sections at two different energies can vary non-trivially with these parameters. If there is no new tensor structure in the HVV couplings, the ratio plots will be flat horizontal curves. Any departure from a horizontal nature of such curves will shed light on new tensor structure in such HVV vertices. The main sources of departure are the interference terms between the SM and HDO contributions. Such terms, occurring in both the numerator and the denominator of the ratio, carry the dependence on f as well as \sqrt{s} .

We also remind the reader that the use of gauge invariant higher-dimensional operators implies a correlated modification in triple gauge boson couplings (Eqs. 6, 7). f_W and f_B are

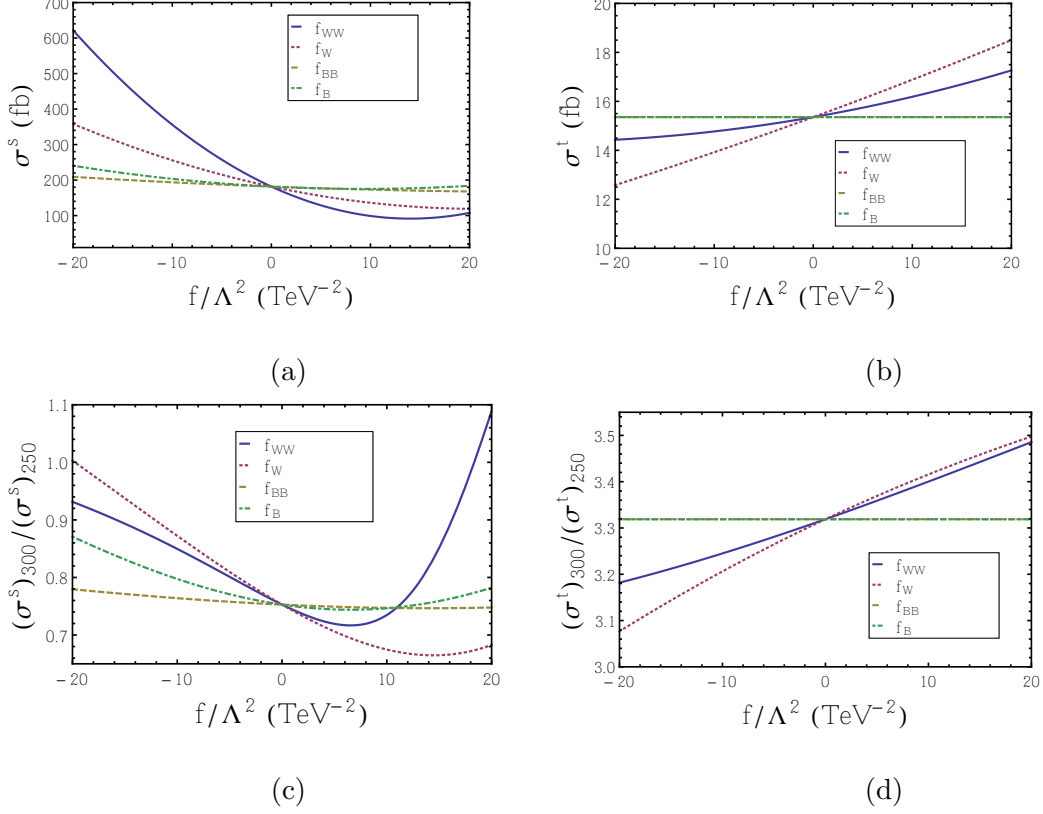


FIG. 5: Variations of (a) $\sigma_{ZH}^s(300)$ (fb) and (c) $\sigma_{ZH}^s(300)/\sigma_{ZH}^s(250)$ for $e^+e^- \rightarrow ZH$ and of (b) $\sigma_{\nu\bar{\nu}H}^{t,ac}(300)$ (fb) and (d) $\sigma_{\nu\bar{\nu}H}^t(300)/\sigma_{\nu\bar{\nu}H}^{t,ac}(250)$ for $e^+e^- \rightarrow \nu\bar{\nu}H$ with f_{WW}, f_W, f_{BB}, f_B . $\kappa = 1$ for all the cases. The superscript *ac* denotes the cut in Eq.10. The numbers in the brackets are the CMEs.

thus responsible for altering the rates of $e^+e^- \rightarrow W^+W^-$ concomitantly with those for Higgs boson production. Such a concomitance, if verified in an e^+e^- collision experiment, should point rather unmistakably at one or the other of the gauge invariant operators mentioned here. We show the modified rates of the WW final state in Fig. 7 where we also show the effects of the operator driven by f_{WWW} (which does not affect the Higgs couplings).

It should however be mentioned that the actual presence of anomalous couplings in $e^+e^- \rightarrow W^+W^-$ is best reflected in a detailed study of various kinematic regions [79]. Such a study, however is not the subject of the present paper.

The main conclusion emerging from Figs. 5, 6 and 7 are as follows :

- In Figs. 5(a) and 6(a), for the process $e^+e^- \rightarrow ZH$, we find that the operator \mathcal{O}_{WW} changes the cross section from its SM expectation by $\sim 30\%$ even in the range $-5 < f_{WW} < 5$. The major contribution to the cross section modification comes from the

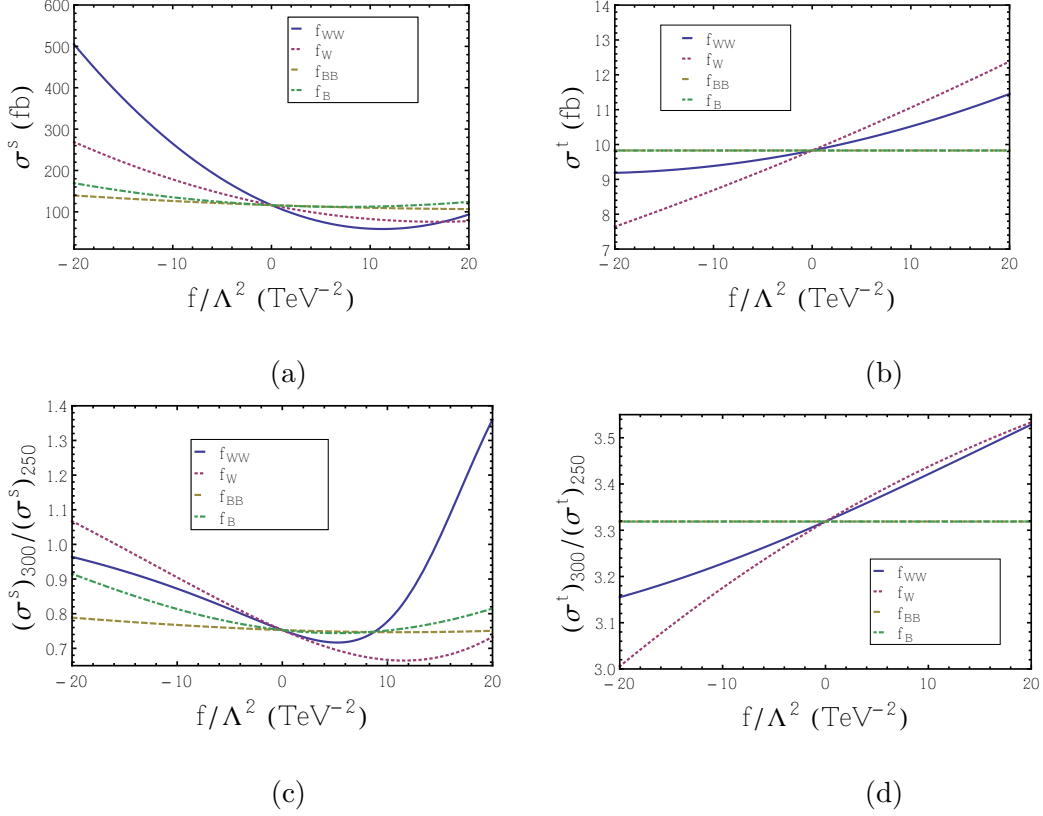


FIG. 6: Variations of (a) $\sigma_{ZH}^s(300)$ (fb) and (c) $\sigma_{ZH}^s(300)/\sigma_{ZH}^s(250)$ for $e^+e^- \rightarrow ZH$ and of (b) $\sigma_{\nu\bar{\nu}H}^{t,ac}(300)$ (fb) and (d) $\sigma_{\nu\bar{\nu}H}^t(300)/\sigma_{\nu\bar{\nu}H}^{t,ac}(250)$ for $e^+e^- \rightarrow \nu\bar{\nu}H$ with f_{WW}, f_W, f_{BB}, f_B . $\kappa = 0.8$ for all the cases. The superscript ac denotes the cut in Eq.10. The numbers in the brackets are the CMEs.

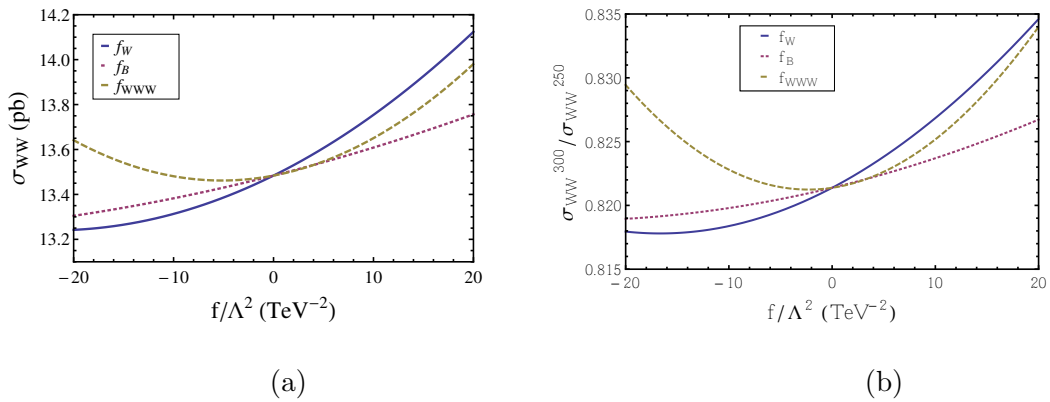


FIG. 7: (a) Cross section (σ in pb) for the process $e^+e^- \rightarrow W^+W^-$ for $\sqrt{s} = 300$ GeV and (b) ratio of cross sections ($\sigma_{300}/\sigma_{250}$) for the same process as functions of f 's.

operators \mathcal{O}_{WW} and \mathcal{O}_W . \mathcal{O}_B and \mathcal{O}_{BB} have lesser contributions to the cross section.

- In Figs. 5(b) and 6(b), for the cut-applied t -channel contribution in the process $e^+e^- \rightarrow \nu\bar{\nu}H$, the operator \mathcal{O}_W maximally affects the cross-section. The effect of \mathcal{O}_{WW} is comparatively less pronounced. \mathcal{O}_{BB} and \mathcal{O}_B does not change this cross-section as the HWW vertex is unaffected by these operators. Most importantly, it should be noted that the effect of these operators on the t -channel process is much less pronounced than its s -channel counterpart (Eqs. 13, 14).
- In Figs. 5(c) and 6(c), the ratio of the cross sections for the $e^+e^- \rightarrow ZH$ channel at $\sqrt{s} = 300$ GeV and $\sqrt{s} = 250$ GeV shows a different nature. In the range $-20 < f_i < 20$ for the four operators discussed above, the ratio changes by $\sim 33\%$ for \mathcal{O}_W . The effect of \mathcal{O}_{WW} is less than this. The change in the ratio is the least for \mathcal{O}_{BB} .
- In Figs. 5(d) and 6(d), the ratio of cross-sections for the cut-applied t -channel process varies in the range $\sim [3.1, 3.5]$ for $-20 < f_i < 20$.
- We see that in Fig. 7, the cross-sections do not vary significantly with the operator coefficients. This is because the $e^+e^- \rightarrow W^+W^-$ channel has a strong ν_e mediated t -channel contribution which does not involve the triple-gauge boson vertex. This has a significant interference with the s -channel. In order to bring out the feature of the triple gauge boson vertices, we need to devise some strategy which will tame down the t -channel effect, such as using right-polarised electrons if one uses a linear collider.

2. Two parameters at the same time

In Figs. 8 and 9, we show some fixed cross-section contours in the planes of two parameters varied at the same time. In Figs.8 and 9, all the parameters apart from the ones shown in the axes, are kept fixed. In each of these figures, we have marked regions in brown where the cross-section is $\sigma(SM) \pm 10\% \times \sigma(SM)$. Hence, we see that for each of these plots, some regions even with large values of the parameters can closely mimic the SM cross-section. The above statement for the ranges of the coefficients of the HDOs will be somewhat modified if we consider the Higgs decays. This is because then we will have branching ratios depending on the effects of the HDOs. Even for fermionic decays of the Higgs, which are independent of the operators under study, the BR will have non-trivial effects on the operator couplings through the total decay width. But, we must mention here that unless we go to very high

values of the operator coefficients, the total decay width remains close to the SM expectation and hence fermionic decay channels would show similar features as these plots. Of course, when we study the effects of all the operators in the basis that we have considered by considering every possible decay mode of the Higgs, then the higher-dimensional operators will come to play at the HVV decay vertices also. Hence, we will get modified bounds on the operator coefficients from a similar approach. We should mention that these operators are also constrained by the electroweak precision observables, *viz.* S , T and U parameters. An important observation which is carried forward from Fig. 5 (a) is that the HZZ and $H\gamma Z$ vertices are very less affected by the operators \mathcal{O}_{BB} and \mathcal{O}_B . This fact is corroborated in Fig.8 (e). The above mentioned pair of operators thus allow a wide region of parameter space which has cross-sections within 10% of the SM value.

Some salient features of Figs. 8 and 9 are :

- Fig. 8 shows the variation of the total rate for the channel $e^+e^- \rightarrow ZH$ as functions of two parameters taken together. All the other parameters are fixed for these plots. In Figs. 8(a)-(d), the cross-section varies significantly from the SM value for the allowed ranges of the parameters. However, Fig. 8(e) shows a large region of the parameter space to have cross-sections similar to the SM (within 10%).
- Fig. 9 shows the variation of the cross-sections for the t -channel process in $e^+e^- \rightarrow \nu\bar{\nu}H$ as functions of two parameters varied at the same time. Figs. 9(c) and 9(d) shows a substantial amount of parameter space agreeing with the SM cross-section.

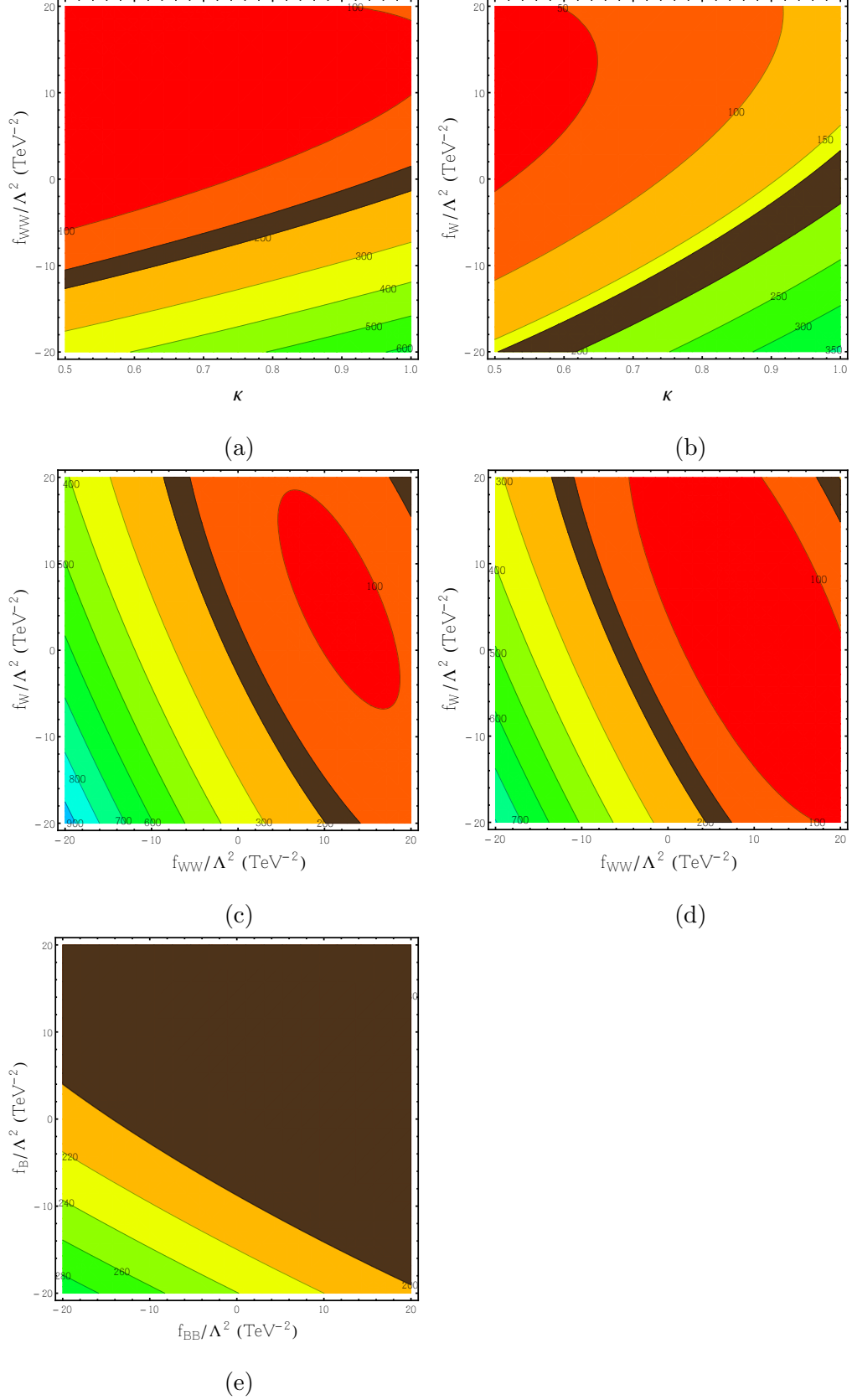


FIG. 8: Variations of σ_s^{300} for $e^+e^- \rightarrow Zh$ with (a) κ and f_{WW} , (b) κ and f_W , (c) f_{WW} and f_W for $\kappa = 1$, (d) f_{WW} and f_W for $\kappa = 0.8$ and (e) f_{BB} and f_B for $\kappa = 1$. For each case all the other f s are set to zeroes. Brown patches signify cross-sections within $\pm 10\%$ of the SM expectation.

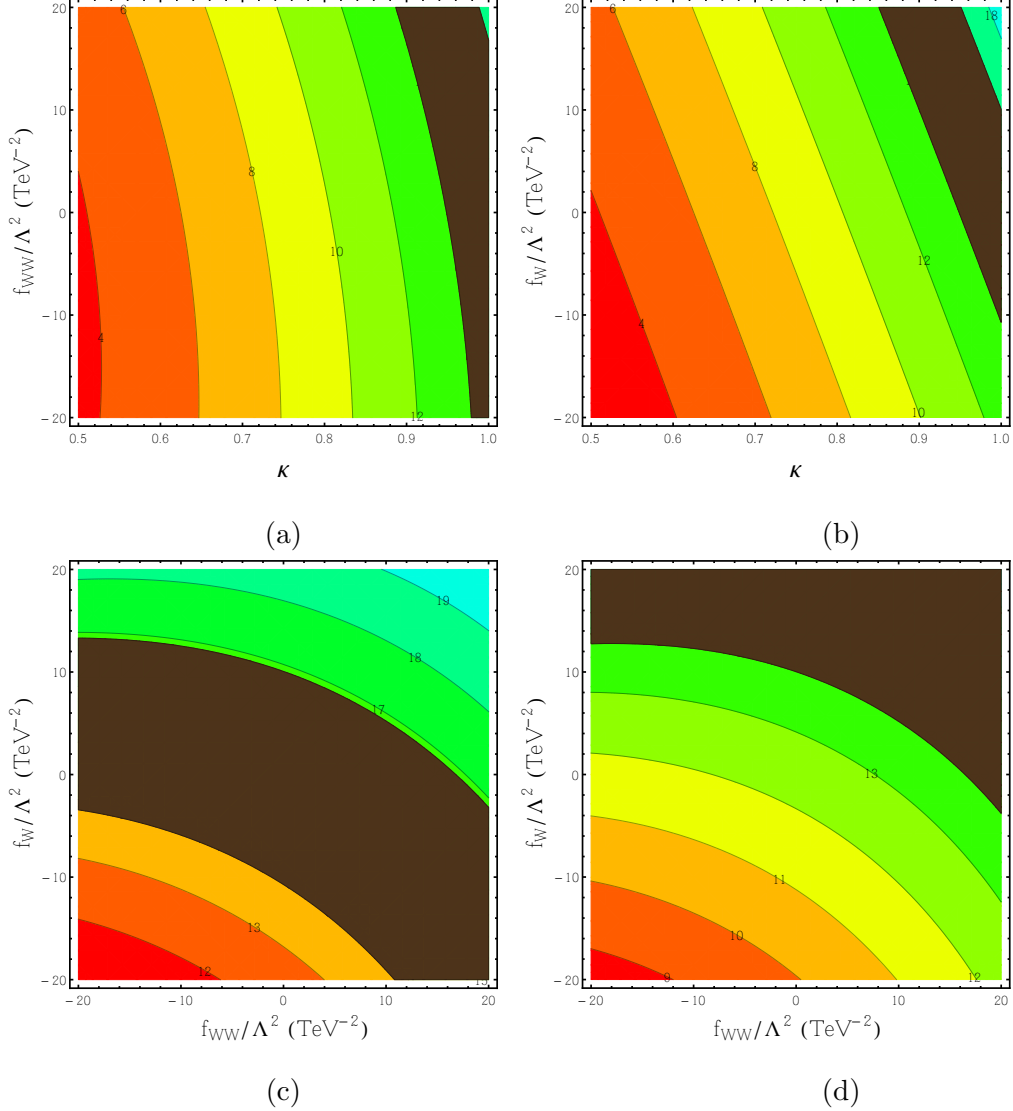


FIG. 9: Variations of $\sigma_t^{300,ac}$ for $e^+e^- \rightarrow Zh$ with (a) κ and f_{WW} , (b) κ and f_W , (c) f_{WW} and f_W for $\kappa = 1$, (d) f_{WW} and f_W for $\kappa = 0.9$. For each case all the other f s are set to zeroes. Brown patches signify cross-sections within $\pm 10\%$ of the SM expectation.

3. All parameters at the same time

The most general case will be to vary all the parameters simultaneously to obtain the most realistic parameter space. Here, we demonstrate this scenario for the cut-applied t -channel cross section in the $e^+e^- \rightarrow \nu\bar{\nu}H$ channel. In Figs.10 (a), (b) and (c) we present three slices of the 3-dimensional hyper-surface. For each of these plots, there is a third parameter which has been varied. We see that a very large parameter space is allowed which can mimic the

SM cross section within its 10% value. Of course these plots are for illustrative purposes only. In Fig. 10 (d), we have shown one such slice of the five-dimensional hyper-surface in the space of $(\kappa, f_{WW}, f_W, f_{BB}$ and $f_B)$ for the s -channel process.

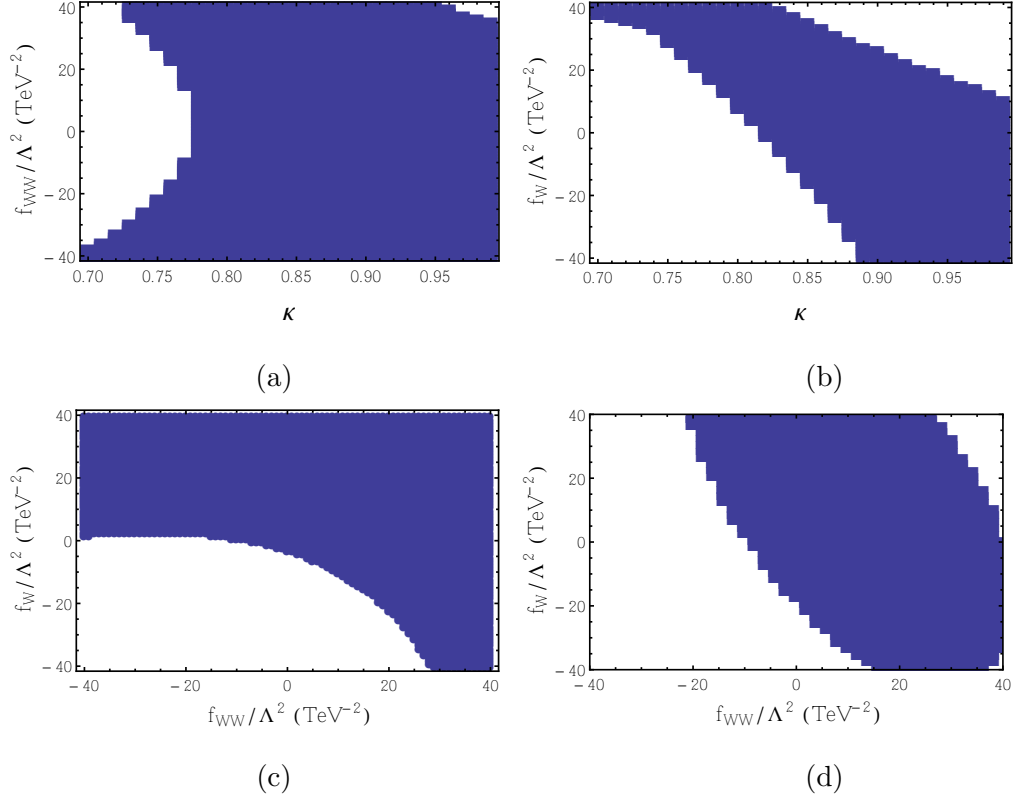


FIG. 10: Allowed parameter space for $\sigma_{\nu\bar{\nu}H}^{t,ac}$ within 10% of its SM value : (a) f_{WW} vs κ (f_W varied), (b) f_W vs κ (f_{WW} varied), (c) f_W vs f_{WW} (κ varied) and for σ_{ZH}^s within 10% of its SM value : (d) f_W vs f_{WW} (κ, f_{BB} and f_B varied). $\sqrt{s} = 300$ GeV.

Discussion on EWPT constraints : All the benchmark points chosen throughout this paper are consistent with all constraints available till date [62, 63]. However, if one looks at the contour plots in Figs. 8, 9 and 10, there may exist certain points which are disfavoured by the precision constraints.

E. The effects on kinematic distributions

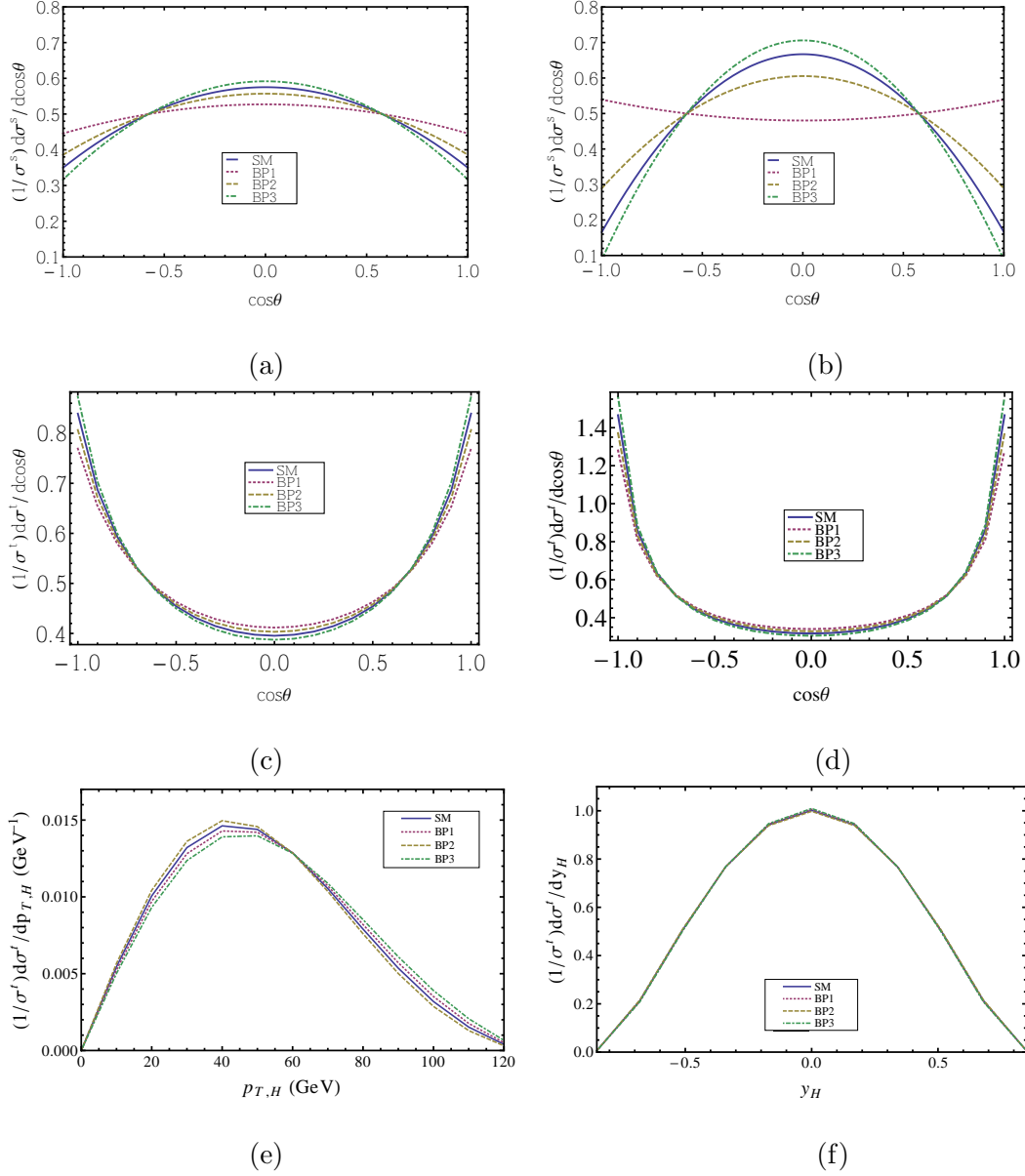


FIG. 11: Normalised kinematic distributions $(1/\sigma^s)d\sigma^s/d\cos\theta$ for the channel $e^+e^- \rightarrow ZH$ for (a) $\sqrt{s} = 300$ GeV and (b) $\sqrt{s} = 500$ GeV. Normalised kinematic distributions $(1/\sigma^t)d\sigma^t/d\cos\theta$ for the t -channel process in $e^+e^- \rightarrow \nu\bar{\nu}H$ for (c) $\sqrt{s} = 300$ GeV and (d) $\sqrt{s} = 500$ GeV. Distributions for (e) $(1/\sigma^t)d\sigma^t/dp_{T,H}$ and (f) $(1/\sigma^t)d\sigma^t/dy_H$ for the t -channel process in $e^+e^- \rightarrow \nu\bar{\nu}H$ at $\sqrt{s} = 300$ GeV. Benchmark points, viz. SM ($x_i \in \{1, 0, 0, 0, 0\}$), BP1 ($x_i \in \{1, -3, 8, -4, 3\}$), BP2 ($x_i \in \{1, 0, 5, 0, 0\}$) and BP3 ($x_i \in \{1, 0, -5, 0, 0\}$).

The presence of anomalous HVV vertex can in principle also affect the shapes of various kinematic distributions. In Figs. 11(a) and 11(b) [Figs. 11(c) and (d)], we show the normalised angular (angle of Higgs with the z -axis) distributions for the s -channel (t -channel) processes for $\sqrt{s} = 300$ GeV and 500 GeV respectively. We find that the angular dependence for the s -channel is very sensitive in some regions of the parameter space allowed by the EWPT constraints and the LHC data. We also find the $\cos\theta$ dependence can be completely opposite as we increase the CME. This can be seen in Figs. 11(a) and 11(b), if we compare the curves for BP1. In contrast, the t -channel is not significantly affected by the inclusion of HDOs. The angular dependence of the differential cross-sections can be expressed as

$$\frac{d\sigma(\sqrt{s}, x_i)}{d\cos\theta} = a(\sqrt{s}, x_i) + b(\sqrt{s}, x_i) \cos^2\theta \quad (16)$$

It is found that, between coefficients a and b above, a is more affected by the anomalous couplings rather than b , unless \sqrt{s} is 500 GeV or well above that. As a result, angular distributions are insensitive to the new interactions at the proposed energy scale of a Higgs factory.

In Figs. 11(e) and 11(f), we show the normalised $d\sigma/dp_{T,h}$ and $d\sigma/dy_h$ distributions respectively for the t -channel where $p_{T,h}$ is the transverse momentum of the Higgs and y_h is its rapidity. We want to emphasise that it is very difficult to see any significant differences in the various kinematic distributions in most of the parameter space allowed by the LHC and EWPT constraints while performing experiments with smaller CME. In both the channels, we do not consider the final decay products of the Higgs. If we consider the Higgs boson decaying to fermionic final states, then the HDOs under consideration will not affect these decay vertices and the above normalised distributions will remain intact. However, if we consider the bosonic decay modes of the Higgs, then the HDOs will affect these distributions non-trivially.

We end this subsection with the following admission. Various kinematical distributions are canonically emphasized as the best places to find the signature of non-standard Lorentz structures in interaction terms. While this expectation is not completely belied in the present case as well, we note that the anomalous couplings are reflected in distributions *at relatively high CMEs*. The reason behind this has already been explained above. While this prospect is encouraging, electron-positron colliders, especially those designed as Higgs factories, are likely to start operating at energies as low as 250 – 300 GeV. Our observation is that the

imprint of anomalous couplings can be found even at such low energies at the level of total rates and their ratios. A detailed study involving all possible decay products and their various correlations can in principle go further in revealing traces of anomalous couplings. We will take up such a study in a subsequent work.

F. Discussion on relevant backgrounds

We wish to see the effects of anomalous HVV couplings on the Higgs production alone. Therefore, we do not look at bosonic decay modes of Higgs and limit our discussion only to those signal processes where H decays maximally to a $b\bar{b}$ pair. For the $e^+e^- \rightarrow ZH$ process, the Z can either decay visibly to $b\bar{b}$, jj , $\ell^+\ell^-$ (here $j = g, u, d, c, s$ and $\ell = e, \mu$) modes or invisibly to a $\nu\bar{\nu}$ pair. So the dominant backgrounds relevant for these final states are the non-Higgs $e^+e^- \rightarrow b\bar{b}b\bar{b}, b\bar{b}jj, b\bar{b}\ell^+\ell^-, b\bar{b} + \cancel{E}$. The non-Higgs $e^+e^- \rightarrow b\bar{b} + \cancel{E}$ process can also act as the dominant background for the $e^+e^- \rightarrow \nu\bar{\nu}H$ channel. We select events after the following kinematic cuts:

Trigger cuts : $p_T(b, j) > 20$ GeV, $p_T(\ell) > 10$ GeV, $|y(b, j)| < 5.0$, $|y(\ell)| < 2.5$, $\Delta R(bb, bj, jj, b\ell, j\ell) > 0.4$, $\Delta R(\ell\ell) > 0.2$.

Finally we estimate two of the aforementioned backgrounds by applying the cuts below:

- Non-Higgs $e^+e^- \rightarrow b\bar{b}\ell\ell$

We demand the two b 's to fall within the Higgs-mass window and the two ℓ 's to fall within the Z -mass window as follows:

$$|M(bb) - M_h| < 10 \text{ GeV} \quad \text{AND} \quad |M(\ell\ell) - M_Z| < 10 \text{ GeV} \quad (17)$$

Finally the total background cross-section for the $b\bar{b}\ell\ell$ final state is defined as, $\mathcal{B}_{b\bar{b}\ell\ell} = \eta_b^2 \sigma_{b\bar{b}\ell\ell}$ where η_b is the b -tagging efficiency which we take as 0.6 for our analysis. The signal is also scaled by the same factor, η_b^2 .

- Non-Higgs $e^+e^- \rightarrow b\bar{b} + \cancel{E}$

We demand the two b 's to fall within the Higgs-mass window, $|M(bb) - M_h| < 10$ GeV. Here the background is $\mathcal{B}_{b\bar{b}+\cancel{E}} = \eta_b^2 \sigma_{b\bar{b}+\cancel{E}}$. The signal³ has also been scaled by

³ The channel $e^+e^- \rightarrow H + \cancel{E} \rightarrow b\bar{b} + \cancel{E}$ also includes diagrams involving the triple-gauge boson vertices. These effects are almost nullified when the selection cuts for this channel are employed.

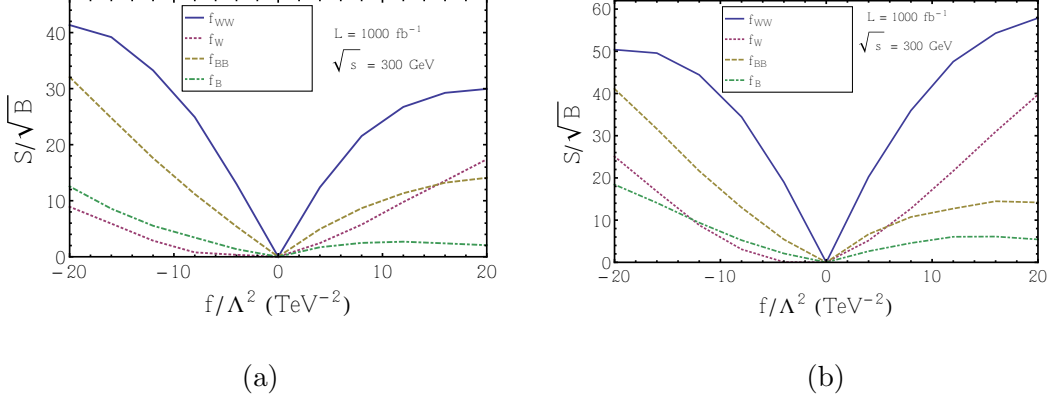


FIG. 12: Significance ($S/\sqrt{\mathcal{B}}$) as functions of f_i/Λ^2 for $\kappa = 1$ at $\sqrt{s} = 300$ GeV for (a) $e^+e^- \rightarrow b\bar{b}l\ell$ and (b) $e^+e^- \rightarrow b\bar{b} + \cancel{E}$.

the b -tagging efficiency.

Final states	\sqrt{s} (GeV)	$\sigma_{SM,tc}^{sig}$ (fb)	$\sigma_{SM,ac}^{sig}$ (fb)	$\sigma_{BP1,tc}^{sig}$ (fb)	$\sigma_{BP1,ac}^{sig}$ (fb)	σ_{tc}^{bkg} (fb)	σ_{ac}^{bkg} (fb)
$b\bar{b}l^+l^-$	250	2.68	2.46	2.76	2.52	10.33	0.09
	300	2.33	1.91	2.31	1.83	9.17	0.07
$b\bar{b} + \cancel{E}$	250	12.25	10.31	12.36	10.53	20.53	0.33
	300	13.67	9.79	13.26	9.62	18.00	0.29

TABLE II: We show the signal and backgrounds for two different final states, *viz.* $b\bar{b}l^+l^-$ and $b\bar{b} + \cancel{E}$. σ_{tc} 's are the cross-sections after the basic trigger cuts mentioned above and σ_{ac} 's are the cross-sections after the channel-specific cuts. The analysis has been done for the SM and the benchmark point BP1 ($x_i \in \{1, -3, 8, -4, 3\}$).

Alongside the issue of distinctness of the presence of the anomalous couplings, it is of interest to find out about the reach of a Higgs factory, or to know down to what strength the anomalous couplings can be detected. This information can be found in Fig. 12. There we have plotted the quantities $\mathcal{S} = |\sigma_{BSM}^H - \sigma_{SM}^H|$ and $\mathcal{B} = \sigma_{SM}^H + \sigma_{SM}^{NH}$ for computing the significance. Here, H (NH) signifies sub-processes which involve (does not involve) the Higgs.

In Table II, we show the cross-sections for both the signal and background scenarios. For the signal we have considered two benchmark points, *viz.* SM and BP1 ($x_i \in$

$\{1, -3, 8, -4, 3\}$). We show the cross-sections once after applying just the trigger cuts (designated with the subscript tc) and next by applying the channel-specific selection cuts (written with a subscript ac) along with the basic trigger cuts. All the numbers have been multiplied by η_b^2 . We see that the effects of the invariant mass selection cuts on the signal cross-sections are negligible whereas these are very effective in reducing the backgrounds almost completely.

The study performed here is at parton level. Shower, hadronization and detector effects are expected to have an impact on the effective cross-sections reported in Table II. That said, these effects will not change the conclusions of the paper.

IV. LIKELIHOOD ANALYSIS FOR t -CHANNEL

The kinematics of the final state associated to the s -channel production has been studied extensively in the past. As pointed out in section I, the t -channel production provides limited phase-space because the momenta of the outgoing neutrinos cannot be disentangled experimentally. This leaves the Higgs boson kinematics as the only handle to explore the nature of the HWW coupling. Studies are documented in the literature with the use of the Higgs boson momentum as a means to gain sensitivity. Here we attempt to fully exploit the kinematics of the Higgs boson by means of a correlated two-dimensional likelihood analysis. The primary intent of this section is to shed light on the relative improvement of this two-dimensional approach, rather than determining absolute sensitivity to the size of anomalous couplings. The latter requires a detailed study that carefully incorporates experimental effects. This is beyond the scope of this paper.

We use a test-statistic (TS) to distinguish the BSM hypothesis from its SM counterpart by defining the logarithm of a profile likelihood ratio ($q_{ij} = \ln \lambda_{ij}$) for two different hypotheses i and j defined as

$$q_{ij} = \ln \lambda_{ij} = \ln \frac{L(P_i|D_i)}{L(P_j|D_i)}, \quad (18)$$

where λ_{ij} is the ratio of two likelihood functions $L(P_i|D_i)$ and $L(P_j|D_i)$ describing two different hypotheses ⁴, D_i is the data set used and $P_{i,j}$ are the probability density functions.

⁴ Alternatively, its reciprocal is also sometimes used, depending on the analysis required. It should be noted here that both likelihoods are constructed using the same D_i , but different P_i s.

Due to the discrete nature of the probabilities in this analysis, the likelihood functions are defined as products of binned Poisson probabilities over all channels and bins [1]. From the TS, a p -value can be calculated to quantify the extent to which a hypothesis can be rejected. In general, a p -value is a portion of the area under a normalised TS which, after calculation, is the percentage confidence level (CL) by which a hypothesis can be rejected.

In Monte Carlo (MC) studies, these TSs emerge as binned peaks which show up on running pseudo-experiments, each of which returns a value for the TS based on a randomly generated set of pseudo-data. The number of pseudo-data points generated is fixed by the cross-section of the process being studied. The TSs concerned in this analysis are always produced in pairs, in order to discriminate between the SM and BSM hypotheses. This pair of TSs is represented as

$$q_U = \ln \frac{L(P_{SM}|D_{SM})}{L(P_{BSM}|D_{SM})} \quad \text{and} \quad q_L = \ln \frac{L(P_{SM}|D_{BSM})}{L(P_{BSM}|D_{BSM})}. \quad (19)$$

The q_U TS tends to have a more positive value due to its ordering, and we refer to it as the *upper* TS for our purposes, while we refer to q_L as the *lower* TS. A hypothesis can be rejected by calculating the associated p -value as follows

$$p = \int_{m_{q_U}}^{\infty} q_L(q) dq, \quad (20)$$

where m_{q_U} is the median of the upper TS, q_U . The confidence by which a hypothesis can be rejected, can alternatively be quantified by knowing the *significance* of the separation between the two TSs. The median-significance, Z_{med} , is defined as the number of standard deviations between the median of q_L and the left edge of the p -value area, that is, the median of q_U .

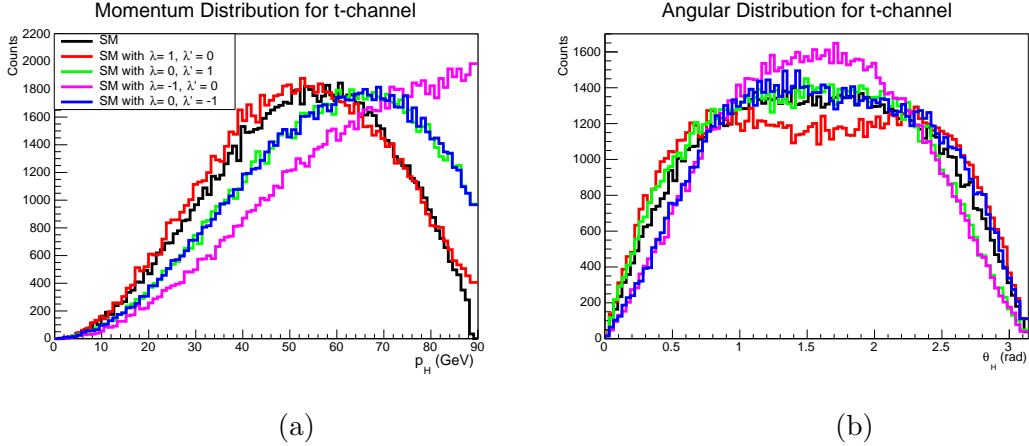


FIG. 13: Normalised kinematic distributions of (a) Higgs momentum, p_H and (b) the angle of the Higgs with the beam-axis, θ_H for different benchmark points for the t -channel process at $\sqrt{s} = 250$ GeV.

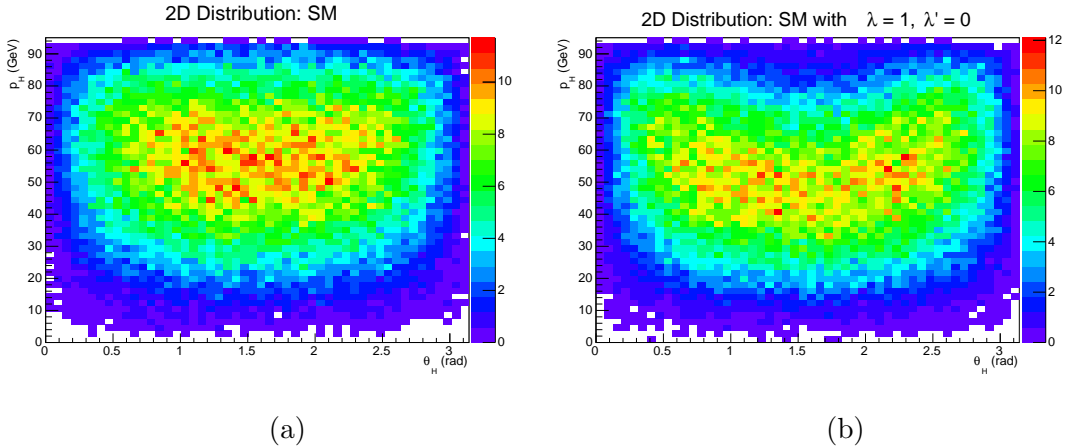


FIG. 14: Two dimensional histograms showing the correlation of the t -channel Higgs momentum, p_H and the angle of the Higgs with the beam-axis, θ_H at $\sqrt{s} = 250$ GeV. The z -axis is an indication of the frequency of events, in arbitrary units. The effect of the correlation can be seen by noting how the BSM parameter λ affects the distribution.

As stated above, we focus on the t -channel process (in $e^+e^- \rightarrow \nu\bar{\nu}H$) which has not been studied as extensively as the s -channel. The s -channel (t -channel) contributions can be separated out from the $\nu\bar{\nu}H$ events by applying the E_H -cut (E_H^c -cut) in Eq. 10. For this purpose, we work with the phenomenological parametrization of anomalous HWW interaction characterised by λ and λ' , as defined in Eq. 9.

In our analysis, the vertices for the Lagrangians in the SM and in BSM with spin-0 bosons

are calculated in FEYNRULES [72] and passed to the event-generator MADGRAPH [74], which is used for the generation of the matrix elements for Higgs production in the t - and s -channels. MC samples are produced at parton level. Effects related to detector resolution are taken into account when defining requirements to suppress the contamination from the s -channel process (see Eq. 10).

We set the stage for the likelihood analysis by showing some plots for distributions in terms of λ and λ' . In Figs. 13(a) and (b), we show the p_H (Higgs momentum) and θ_H (the angle of the Higgs with the beam-axis) distributions respectively for the t -channel at $\sqrt{s} = 250$ GeV. We see that significant deviations from the SM can be seen. This is in contrast to what was shown for the gauge invariant formulation (in Fig. 11) because there we stick to moderate values of the parameter coefficients, whereas for example, here, $\{\lambda = 1, \lambda' = 0\} \Rightarrow x_i \approx \{1, 77, 0, 0, 0\}$. In Figs. 14(a) and (b), two dimensional histograms in p_H - θ_H plane are shown for the SM and a BSM (SM with $\lambda = 1, \lambda' = 0$) benchmark point respectively at $\sqrt{s} = 250$ GeV.

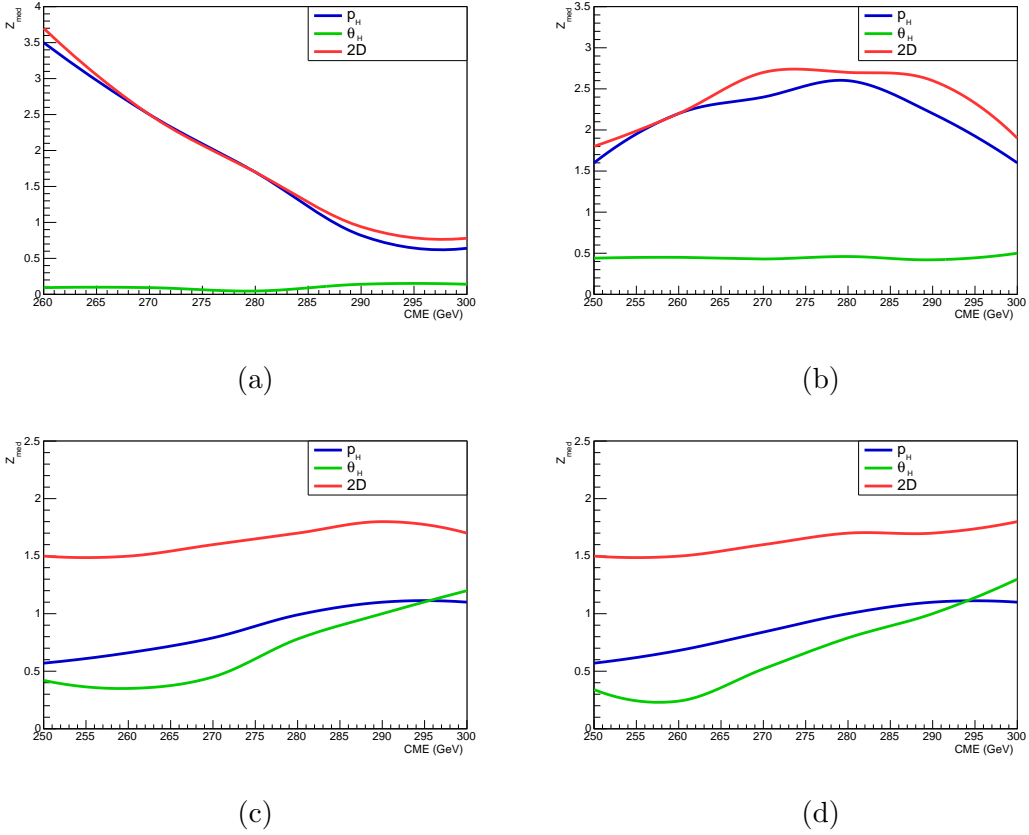


FIG. 15: Median significance values for likelihood analyses done with both one dimensional and two dimensional distributions. (a) SM with $\lambda = 1$, (b) SM with $\lambda = -1$, (c) SM with $\lambda' = 1$ and (d) SM with $\lambda' = -1$. Results are obtained with 1 fb^{-1} of integrated luminosity.

A likelihood analysis for each BSM hypothesis is performed for integrated luminosities of 1 fb^{-1} , 5 fb^{-1} and 10 fb^{-1} . The number of pseudo-data points in each analysis is determined from the SM cross section. The Z_{med} for the 1 fb^{-1} case are plotted as functions of the CME for each hypothesis as shown in Fig. 15. These plots show the power of using two dimensional distributions in likelihood analysis. The likelihood analysis is performed using a total number of 100,000 pseudo-experiments for each TS. The two dimensional distributions, examples of which are shown in Fig. 14, are also included in the likelihood analysis to demonstrate the effect of the correlation between the two variables, p_H and θ_H .

Fig. 15 displays the significance for one-dimensional analyses using the Higgs boson momentum and the polar angle separately. Results are shown for illustration purposes for 1 fb^{-1} of integrated luminosity. Conclusions drawn here are found not to depend on the integrated luminosity in the range studied here. The corresponding results for the combined 2D likeli-

hood are shown. The upper two plots correspond to admixtures with the CP-even term. The sensitivity of the polar angle is significantly less than that of the Higgs boson momentum. The lower plots display the corresponding results for admixtures with the CP-odd term. In this case the sensitivity of the polar angle is similar to that of the momentum. As a result, the improvement from the 2D analysis is significant, to the extent that the sensitivity can be enhanced by about a factor of two. The sensitivity of the angular variable grows with the CME.

The results provide a good motivation for the role of an electron positron collider in understanding the nature of the HVV couplings. The plots in Fig. 15 show the utility in using two dimensional distributions in discerning the rejection of hypotheses. That is, using the same accrued data from two separate one dimensional distributions, one can enhance the confidence in rejecting hypotheses. The correlation of the two dimensional distributions thus carries vital information about the dynamics of the processes which are studied in e^+e^- collisions.

V. SUMMARY AND CONCLUSIONS

We have attempted to demonstrate the efficacy as well as limitations of an e^+e^- Higgs factory operating at 250 – 300 GeV in probing anomalous, higher-dimensional couplings of a Higgs to W -and Z -pairs, suppressed by a scale $\mathcal{O}(\text{TeV})$. For this purpose, we have mostly adhered to the set of gauge-invariant operators that can lead to such interactions, since it is such terms that are expected to emerge on integrating out physics above the electroweak symmetry breaking scale. We have utilised the consequent correlation of the anomalous HWW , HZZ and $HZ\gamma$ couplings, and also the concomitant effect on $ZWW/\gamma WW$ interactions, as reflected in gauge boson pair-production rates.

The general conclusion reached by this study is that the total rates can be quite useful as probes of higher-dimensional operators. Based on this, we have performed a detailed analysis of the cross-sections for s -and t -channel Higgs production, specifying event selection criteria for minimising their mutual contamination. A general scheme of computing the rates with more than one gauge-invariant operators has been outlined. Based on such an analysis, we conclude that, even with the additional operators well within the erstwhile experimental bounds (including those from the LHC), a number of observations can probe them at a

Higgs factory. These include not only the individual total cross-sections but also their ratios at different values of \sqrt{s} and also the ratio of the s - and the t -channel Higgs production rates at fixed energies. We also indicate the correlated variation of W -pair production rates. The Higgs production rate contours with more than one type of anomalous gauge-invariant operators are also presented. Finally, using some illustrative values of anomalous HWW couplings in a more phenomenological parametrization, we indicate the viability of a correlated two-dimensional likelihood analysis to fully exploit the kinematics of the Higgs boson. The latter is particularly relevant to disentangle the SM from CP-violating admixtures. On the whole, we thus conclude that a Higgs factory can considerably improve our understanding of whether the recently discovered scalar is the SM Higgs or not, as evinced from its interactions with a pair of weak gauge bosons.

Acknowledgements

We thank Taushif Ahmed, Satyanarayan Mukhopadhyay and Narayan Rana for helpful discussions. The work done by SvB was supported by The Claude Leon Foundation. The work of S.B., T.M. and B. Mukhopadhyaya was partially supported by funding available from the Department of Atomic Energy, Government of India for the Regional Centre for Accelerator-based Particle Physics (RECAPP), Harish-Chandra Research Institute. B. Mel-lado acknowledges the hospitality of RECAPP, Harish-Chandra Research Institute, during the collaboration.

-
- [1] G. Aad *et al.* [ATLAS Collaboration], Phys. Lett. B **716**, 1 (2012) [arXiv:1207.7214 [hep-ex]].
 - [2] S. Chatrchyan *et al.* [CMS Collaboration], Phys. Lett. B **716**, 30 (2012) [arXiv:1207.7235 [hep-ex]].
 - [3] S. L. Glashow, Nucl. Phys. **22**, 579 (1961).
 - [4] S. Weinberg, Phys. Rev. Lett. **19**, 1264 (1967).
 - [5] N. Svartholm, ed.. 8th Nobel Symposium, C68-05-19 (1968).
 - [6] F. Englert and R. Brout, Phys. Rev. Lett. **13**, 321 (1964).
 - [7] P. W. Higgs, Phys. Rev. Lett. **13**, 508 (1964).
 - [8] P. W. Higgs, Phys. Lett. **12**, 132 (1964).

- [9] P. W. Higgs, Phys. Rev. **145**, 1156 (1966).
- [10] G. S. Guralnik, C. R. Hagen and T. W. B. Kibble, Phys. Rev. Lett. **13**, 585 (1964).
- [11] T. W. B. Kibble, Phys. Rev. **155**, 1554 (1967).
- [12] F. Bonnet, M. B. Gavela, T. Ota and W. Winter, Phys. Rev. D **85**, 035016 (2012) [arXiv:1105.5140 [hep-ph]].
- [13] J. R. Espinosa, C. Grojean, M. Muhlleitner and M. Trott, JHEP **1205**, 097 (2012) [arXiv:1202.3697 [hep-ph]].
- [14] P. P. Giardino, K. Kannike, M. Raidal and A. Strumia, JHEP **1206**, 117 (2012) [arXiv:1203.4254 [hep-ph]].
- [15] T. Li, X. Wan, Y. k. Wang and S. h. Zhu, JHEP **1209**, 086 (2012) [arXiv:1203.5083 [hep-ph]].
- [16] M. Rauch, arXiv:1203.6826 [hep-ph].
- [17] J. R. Espinosa, M. Muhlleitner, C. Grojean and M. Trott, JHEP **1209**, 126 (2012) [arXiv:1205.6790 [hep-ph]].
- [18] J. Ellis and T. You, JHEP **1206**, 140 (2012) [arXiv:1204.0464 [hep-ph]].
- [19] D. Carmi, A. Falkowski, E. Kuflik and T. Volansky, JHEP **1207**, 136 (2012) [arXiv:1202.3144 [hep-ph]].
- [20] M. Duhrssen, S. Heinemeyer, H. Logan, D. Rainwater, G. Weiglein and D. Zeppenfeld, Phys. Rev. D **70**, 113009 (2004) [hep-ph/0406323].
- [21] R. Lafaye, T. Plehn, M. Rauch, D. Zerwas and M. Duhrssen, JHEP **0908**, 009 (2009) [arXiv:0904.3866 [hep-ph]].
- [22] N. Desai, D. K. Ghosh and B. Mukhopadhyaya, Phys. Rev. D **83**, 113004 (2011) [arXiv:1104.3327 [hep-ph]].
- [23] M. Klute, R. Lafaye, T. Plehn, M. Rauch and D. Zerwas, Phys. Rev. Lett. **109**, 101801 (2012) [arXiv:1205.2699 [hep-ph]].
- [24] A. Azatov, R. Contino, D. Del Re, J. Galloway, M. Grassi and S. Rahatlou, JHEP **1206**, 134 (2012) [arXiv:1204.4817 [hep-ph]].
- [25] I. Low, J. Lykken and G. Shaughnessy, Phys. Rev. D **86**, 093012 (2012) [arXiv:1207.1093 [hep-ph]].
- [26] T. Corbett, O. J. P. Eboli, J. Gonzalez-Fraile and M. C. Gonzalez-Garcia, Phys. Rev. D **86**, 075013 (2012) [arXiv:1207.1344 [hep-ph]].
- [27] P. P. Giardino, K. Kannike, M. Raidal and A. Strumia, Phys. Lett. B **718**, 469 (2012)

- [arXiv:1207.1347 [hep-ph]].
- [28] J. Baglio, A. Djouadi and R. M. Godbole, *Phys. Lett. B* **716**, 203 (2012) [arXiv:1207.1451 [hep-ph]].
- [29] J. Ellis and T. You, *JHEP* **1209**, 123 (2012) [arXiv:1207.1693 [hep-ph]].
- [30] M. Montull and F. Riva, *JHEP* **1211**, 018 (2012) [arXiv:1207.1716 [hep-ph]].
- [31] J. R. Espinosa, C. Grojean, M. Muhlleitner and M. Trott, *JHEP* **1212**, 045 (2012) [arXiv:1207.1717 [hep-ph]].
- [32] D. Carmi, A. Falkowski, E. Kuflik, T. Volansky and J. Zupan, *JHEP* **1210**, 196 (2012) [arXiv:1207.1718 [hep-ph]].
- [33] S. Banerjee, S. Mukhopadhyay and B. Mukhopadhyaya, *JHEP* **1210**, 062 (2012) [arXiv:1207.3588 [hep-ph]].
- [34] F. Bonnet, T. Ota, M. Rauch and W. Winter, *Phys. Rev. D* **86**, 093014 (2012) [arXiv:1207.4599 [hep-ph]].
- [35] T. Plehn and M. Rauch, *Europhys. Lett.* **100**, 11002 (2012) [arXiv:1207.6108 [hep-ph]].
- [36] A. Djouadi, *Eur. Phys. J. C* **73**, 2498 (2013) [arXiv:1208.3436 [hep-ph]].
- [37] B. Batell, S. Gori and L. T. Wang, *JHEP* **1301**, 139 (2013) [arXiv:1209.6382 [hep-ph]].
- [38] G. Moreau, *Phys. Rev. D* **87**, 015027 (2013) [arXiv:1210.3977 [hep-ph]].
- [39] G. Bhattacharyya, D. Das and P. B. Pal, *Phys. Rev. D* **87**, 011702 (2013) [arXiv:1212.4651 [hep-ph]].
- [40] D. Choudhury, R. Islam and A. Kundu, *Phys. Rev. D* **88**, no. 1, 013014 (2013) [arXiv:1212.4652 [hep-ph]].
- [41] G. Belanger, B. Dumont, U. Ellwanger, J. F. Gunion and S. Kraml, *JHEP* **1302**, 053 (2013) [arXiv:1212.5244 [hep-ph]].
- [42] M. Klute, R. Lafaye, T. Plehn, M. Rauch and D. Zerwas, *Europhys. Lett.* **101**, 51001 (2013) [arXiv:1301.1322 [hep-ph]].
- [43] C. Grojean, E. E. Jenkins, A. V. Manohar and M. Trott, *JHEP* **1304**, 016 (2013) [arXiv:1301.2588 [hep-ph]].
- [44] K. Cheung, J. S. Lee and P. Y. Tseng, *JHEP* **1305**, 134 (2013) [arXiv:1302.3794 [hep-ph]].
- [45] J. Elias-Mir, J. R. Espinosa, E. Masso and A. Pomarol, *JHEP* **1308**, 033 (2013) [arXiv:1302.5661 [hep-ph]].
- [46] J. Ellis, V. Sanz and T. You, *Eur. Phys. J. C* **73**, 2507 (2013) [arXiv:1303.0208 [hep-ph]].

- [47] P. P. Giardino, K. Kannike, I. Masina, M. Raidal and A. Strumia, *JHEP* **1405**, 046 (2014) [arXiv:1303.3570 [hep-ph]].
- [48] R. Contino, M. Ghezzi, C. Grojean, M. Muhlleitner and M. Spira, *JHEP* **1307**, 035 (2013) [arXiv:1303.3876 [hep-ph]].
- [49] J. Ellis and T. You, *JHEP* **1306**, 103 (2013) [arXiv:1303.3879 [hep-ph]].
- [50] A. Djouadi and G. Moreau, *Eur. Phys. J. C* **73**, 2512 (2013) [arXiv:1303.6591 [hep-ph]].
- [51] W. F. Chang, W. P. Pan and F. Xu, *Phys. Rev. D* **88**, no. 3, 033004 (2013) [arXiv:1303.7035 [hep-ph]].
- [52] T. Corbett, O. J. P. boli, J. Gonzalez-Fraile and M. C. Gonzalez-Garcia, *Phys. Rev. Lett.* **111**, no. 1, 011801 (2013) [arXiv:1304.1151 [hep-ph]].
- [53] B. Dumont, S. Fichet and G. von Gersdorff, *JHEP* **1307**, 065 (2013) [arXiv:1304.3369 [hep-ph]].
- [54] J. Elias-Miro, J. R. Espinosa, E. Masso and A. Pomarol, *JHEP* **1311**, 066 (2013) [arXiv:1308.1879 [hep-ph]].
- [55] M. B. Einhorn and J. Wudka, *Nucl. Phys. B* **877**, 792 (2013) [arXiv:1308.2255 [hep-ph]].
- [56] A. Pomarol and F. Riva, *JHEP* **1401**, 151 (2014) [arXiv:1308.2803 [hep-ph]].
- [57] G. Aad *et al.* [ATLAS Collaboration], *Phys. Rev. Lett.* **112**, 201802 (2014) [arXiv:1402.3244 [hep-ex]].
- [58] M. E. Chasco [CMS Collaboration], arXiv:1310.1002 [hep-ex].
- [59] T. Han and B. Mellado, *Phys. Rev. D* **82**, 016009 (2010)
- [60] S. S. Biswal, R. M. Godbole, B. Mellado and S. Raychaudhuri, *Phys. Rev. Lett.* **109**, 261801 (2012) [arXiv:1203.6285 [hep-ph]].
- [61] S. S. Biswal, R. M. Godbole, R. K. Singh and D. Choudhury, *Phys. Rev. D* **73**, 035001 (2006) [Erratum-*ibid.* *D* **74**, 039904 (2006)] [hep-ph/0509070].
- [62] T. Corbett, O. J. P. boli, J. Gonzalez-Fraile and M. C. Gonzalez-Garcia, arXiv:1306.0006 [hep-ph].
- [63] E. Masso and V. Sanz, *Phys. Rev. D* **87**, no. 3, 033001 (2013) [arXiv:1211.1320 [hep-ph]].
- [64] T. Corbett, O. J. P. Eboli, J. Gonzalez-Fraile and M. C. Gonzalez-Garcia, *Phys. Rev. D* **87**, 015022 (2013) [arXiv:1211.4580 [hep-ph]].
- [65] A. Falkowski, F. Riva and A. Urbano, *JHEP* **1311**, 111 (2013) [arXiv:1303.1812 [hep-ph]].
- [66] S. Banerjee, S. Mukhopadhyay and B. Mukhopadhyaya, *Phys. Rev. D* **89**, 053010 (2014)

- [arXiv:1308.4860 [hep-ph]].
- [67] W. Buchmuller and D. Wyler, Nucl. Phys. B **268**, 621 (1986).
- [68] B. Grzadkowski, M. Iskrzynski, M. Misiak and J. Rosiek, JHEP **1010**, 085 (2010) [arXiv:1008.4884 [hep-ph]].
- [69] K. Hagiwara, R. Szalapski and D. Zeppenfeld, Phys. Lett. B **318**, 155 (1993) [hep-ph/9308347].
- [70] M. C. Gonzalez-Garcia, Int. J. Mod. Phys. A **14**, 3121 (1999) [hep-ph/9902321].
- [71] A. Djouadi, R. M. Godbole, B. Mellado and K. Mohan, Phys. Lett. B **723**, 307 (2013) [arXiv:1301.4965 [hep-ph]].
- [72] A. Alloul, N. D. Christensen, C. Degrande, C. Duhr and B. Fuks, Comput. Phys. Commun. **185**, 2250 (2014) [arXiv:1310.1921 [hep-ph]].
- [73] C. Degrande, C. Duhr, B. Fuks, D. Grellscheid, O. Mattelaer and T. Reiter, Comput. Phys. Commun. **183**, 1201 (2012) [arXiv:1108.2040 [hep-ph]].
- [74] J. Alwall, M. Herquet, F. Maltoni, O. Mattelaer and T. Stelzer, JHEP **1106**, 128 (2011) [arXiv:1106.0522 [hep-ph]].
- [75] J. A. M. Vermaseren, math-ph/0010025.
- [76] S. Heinemeyer, S. Kanemura, H. Logan, A. Raspereza, T. M. P. Tait, H. Baer, E. L. Berger and A. Birkedal *et al.*, hep-ph/0511332.
- [77] G. Altarelli, B. Mele and F. Pitolli, Nucl. Phys. B **287**, 205 (1987).
- [78] Private communications with Alex Pomarol, Dieter Zeppenfeld and Maxim Perelstein.
- [79] K. Hagiwara, R. D. Peccei, D. Zeppenfeld and K. Hikasa, Nucl. Phys. B **282**, 253 (1987).